Factors regulating the Great Calcite Belt in the Southern Ocean and its biogeochemical significance: Regulation of the Great Calcite Belt

Article *in* Global Biogeochemical Cycles · June 2016

DOI: 10.1002/2016GB005414

CITATIONS
35

READS
246

11 authors, including:

William Balch
Bigelow Laboratory for Ocean Sciences
1,759 PUBLICATIONS **6,818** CITATIONS
SEE PROFILE

Nicholas R. Bates
Bermuda Institute of Ocean Sciences
300 PUBLICATIONS **13,745** CITATIONS
SEE PROFILE

Phoebe J. Lam
University of California, Santa Cruz
58 PUBLICATIONS **2,583** CITATIONS
SEE PROFILE

Benjamin S Twining
Bigelow Laboratory for Ocean Sciences
100 PUBLICATIONS **3,481** CITATIONS
SEE PROFILE

AGU PUBLICATIONS

Global Biogeochemical Cycles

RESEARCH ARTICLE
10.1002/2016GB005414

Key Points:
- The Southern Ocean Great Calcite Belt (GCB) results from high coccolithophore abundance
- The Great Calcite Belt enhances the ocean source of CO_2 and increases the POC transfer efficiency
- The formation of the Great Calcite Belt is driven by macronutrient and micronutrient effects on phytoplankton growth

Correspondence to:
W. M. Balch,
bbalch@bigelow.org

Citation:
Balch, W. M., et al. (2016), Factors regulating the Great Calcite Belt in the Southern Ocean and its biogeochemical significance, *Global Biogeochem. Cycles*, *30*, doi:10.1002/2016GB005414.

Received 28 MAR 2016
Accepted 23 MAY 2016
Accepted article online 6 AUG 2016

Factors regulating the Great Calcite Belt in the Southern Ocean and its biogeochemical significance

William M. Balch[1], Nicholas R. Bates[2,3], Phoebe J. Lam[4,5], Benjamin S. Twining[1], Sarah Z. Rosengard[4,6], Bruce C. Bowler[1], Dave T. Drapeau[1], Rebecca Garley[2], Laura C. Lubelczyk[1], Catherine Mitchell[1], and Sara Rauschenberg[1]

[1]Bigelow Laboratory for Ocean Sciences, East Boothbay, Maine, USA, [2]Bermuda Institute of Ocean Sciences (BIOS), Inc., St. George, Bermuda, [3]Department of Ocean and Earth Sciences, University of Southampton, Southampton, UK, [4]Department of Marine Chemistry and Geochemistry, Woods Hole Oceanographic Institution, Woods Hole, Massachusetts, USA, [5]Now at Department of Ocean Sciences, University of California, Santa Cruz, California, USA, [6]Massachusetts Institute of Technology, Cambridge, Massachusetts, USA

Abstract The Great Calcite Belt (GCB) is a region of elevated surface reflectance in the Southern Ocean (SO) covering ~16% of the global ocean and is thought to result from elevated, seasonal concentrations of coccolithophores. Here we describe field observations and experiments from two cruises that crossed the GCB in the Atlantic and Indian sectors of the SO. We confirm the presence of coccolithophores, their coccoliths, and associated optical scattering, located primarily in the region of the subtropical, Agulhas, and Subantarctic frontal regions. Coccolithophore-rich regions were typically associated with high-velocity frontal regions with higher seawater partial pressures of CO_2 (pCO_2) than the atmosphere, sufficient to reverse the direction of gas exchange to a CO_2 source. There was no calcium carbonate ($CaCO_3$) enhancement of particulate organic carbon (POC) export, but there were increased POC transfer efficiencies in high-flux particulate inorganic carbon regions. Contemporaneous observations are synthesized with results of trace-metal incubation experiments, ^{234}Th-based flux estimates, and remotely sensed observations to generate a mandala that summarizes our understanding about the factors that regulate the location of the GCB.

1. Introduction

The pool of particulate inorganic carbon (PIC) is an important reservoir for carbon in the global ocean, with its rates of production, storage, and export providing complex feedback to the global ocean carbon cycle. Estimates of annual PIC production are highly unconstrained, ranging from ~0.4 to 1.8 Pg C yr^{-1} based on ocean sediment trap estimates [*Balch et al.*, 2007; *Berelson et al.*, 2007; *Feely et al.*, 2004; *Milliman*, 1993; *Morse and Mackenzie*, 1990; *Wollast*, 1994]. Other observational approaches such as satellite remote sensing of PIC [*Balch et al.*, 2005; *Iglesias-Rodríguez et al.*, 2002; *Moore et al.*, 2012], modeling [*Pinsonneault et al.*, 2012], and global alkalinity tracer variability [e.g., *Fry et al.*, 2015] offer further evidence on the location, timing, and magnitude of PIC production, PIC to organic carbon rain ratio, and contributions to the global carbon cycle. The aim of these approaches is to elucidate the climate change-ocean acidification feedback on calcium carbonate ($CaCO_3$) production and dissolution [*Ridgwell et al.*, 2007; *Riebesell et al.*, 2000; *Zondervan et al.*, 2001] and ultimately carbonate-organic matter ballasting of anthropogenic CO_2 [*Tanhua et al.*, 2013].

Satellite observations enable quantitative estimates of coccolithophore PIC concentrations in the upper ocean through remote sensing algorithms [*Balch et al.*, 2005; *Gordon et al.*, 2001]. The PIC algorithm has been validated previously, mostly in the North Atlantic Ocean. In the Southern Ocean, satellite-derived PIC concentrations suggest that a substantive region of elevated PIC, previously defined as the Great Calcite Belt (GCB) [*Balch et al.*, 2011], occurs each year in the austral summer near the Subtropical Front (STF), Subantarctic Front (SAF), and Polar Front (PF). The GCB appears seasonally in austral summer south of ~38°S and extends poleward to ~60°S with an area of ~52×10^6 km^2. Ship observations have confirmed that the brightest, highest PIC concentrations are found northeast of the Drake Passage, in the region of the Patagonian Shelf and Falkland Islands [*Balch et al.*, 2014b; *Garcia et al.*, 2011; *Painter et al.*, 2010; *Poulton et al.*, 2013]. Satellite-derived PIC concentrations gradually diminish eastward, remaining discernable throughout the Indian and Pacific sectors of the Southern Ocean (SO).

Satellite estimates indicate that 26% of global suspended PIC is found in the GCB, which represents 16% of the global ocean by area [*Balch et al.*, 2005]. This would suggest that the GCB is arguably the largest ocean

coccolithophore-rich biome. Indeed, supporting evidence of its presence (and domination by the coccolithophore, *Emiliania huxleyi*) has been observed in seawater samples across all sectors of the SO, as far south as 65°S with shipboard observations since the 1960s [see *Holligan et al*., 2010, their Table 1].

1.1. The Role of Bottom-Up Nutrient Supply on Coccolithophore Production

The spatiotemporal success of one algal group over another group in the GCB is likely related to physical and biogeochemical factors involving the bottom-up supply of nutrients or top-down grazing. Significant portions of the SO in the region of the GCB are considered high nutrient, low chlorophyll (HNLC) [*Minas and Minas*, 1992], with abundant macronutrients and limiting iron [*Boyd et al*., 1999]. Diatoms usually require $Si(OH)_4$ and NO_3 in roughly equal portions [*Brzezinski*, 1985]. Typically, if diatom growth becomes limited by Si (concentrations $< \sim 2\,\mu M$), non-Si users are able to grow faster [*Dugdale and MacIsacc*, 1971; *Egge and Aksnes*, 1992] and can dominate. Moreover, simulation models have suggested that when $Si(OH)_4$ reaches a critical, low concentration, coccolithophorids can dominate [*Aksnes et al*., 1994].

Iron availability also influences phytoplankton growth and community structure in large sectors of the ocean [*Boyd et al*., 2007; *Moore et al*., 2013], and this, indeed, may influence the GCB. Although coccolithophores generally appear less prone to iron limitation compared to diatoms and other microplankton [*Brand*, 1991; *Lam et al*., 2001; *Sunda and Huntsman*, 1995], iron has been reported to limit coccolithophore growth in regions of the North Atlantic and Pacific Oceans [*Crawford et al*., 2003; *Nielsdottir et al*., 2009]. In the southern hemisphere, higher PIC concentrations are found near continental landmasses and islands, suggesting that associated trace metal supply (either aeolian or upwelled) may help support seasonal coccolithophore production. Furthermore, strong correlations have been noted in sediment records from the SAF zone between fluxes of dust and alkenones (coccolithophore biomarkers) on glacial time scales [*Jaccard et al*., 2013; *Martínez-Garcia et al*., 2009, 2014], suggesting that coccolithophores are stimulated by nutrients from dust.

The co-location of the GCB with major oceanographic fronts would suggest that bottom-up supply of upwelled nutrients along these frontal boundaries plays a dominant role in controlling coccolithophore productivity. Because of the importance of nitrate and silicate for phytoplankton growth, several indices have been used to describe their covariability (or lack thereof) in the sea. The Si:N ratio reveals the relative overabundance of silicate in deep waters of the SO [*Sarmiento et al*., 2007] associated with differences in remineralization of nitrate and silicate and effects of iron on sinking particulate Si and N. Residual nitrate (nitrate–silicate) also has been used to describe the fertility of water masses in coastal waters such as the Gulf of Maine for supporting diatoms versus nonsiliceous phytoplankton [*Townsend et al*., 2010]. Specifically, in HNLC waters such as the SO, the issue for either of these indices is that for understanding the potential effect of nitrate and silicate on phytoplankton growth, an index is needed that scales the dominant nutrient concentration to the potential growth that they could sustain should growth limitation (e.g., by a trace metal) be removed.

1.2. The Role of the GCB on the Dissolved Inorganic Carbon Cycle and Export Ratio

The seasonal presence of the GCB in the Southern Ocean may have substantive implications for carbon biogeochemistry in the region [*Freeman and Lovenduski*, 2015]. The distribution of coccolithophores in the GCB may affect the efficiency of the biological carbon pump in two opposing ways: (1) as part of the carbonate (PIC) pump, lowering total alkalinity (TA) in the surface ocean during calcification and thereby *increasing* seawater pCO_2 via changes in CO_2-carbonate equilibria [e.g., *Bates et al*., 1996a; *Zeebe and Wolf-Gladrow*, 2001], and (2) through a ballasting effect that increases the magnitude and/or transfer efficiency of the soft tissue (particulate organic carbon (POC)) pump, which would *decrease* surface ocean pCO_2 [e.g., *Tanhua et al*., 2013, and references within]. The balance of the POC and PIC pumps determines the net effect of the biological carbon pump on surface pCO_2, exchanges of CO_2 across the air-sea interface, and ultimately feeds back to atmospheric pCO_2. Model studies have shown that atmospheric CO_2 is highly sensitive to the PIC:POC export ratio [*Archer and Maier-Reimer*, 1994; *Archer et al*., 2000; *Matsumoto et al*., 2002], particularly in the SO. Halving the global PIC:POC export ratio can lead to an atmospheric CO_2 decrease of 55 ppm [*Sigman et al*., 1998]. Despite the importance of the PIC:POC export ratio, however, its magnitude is not well constrained. *Sarmiento et al.* [2002] argued that the often-used global PIC:POC export ratio of 0.25 [*Archer et al*., 2000] is too high. They calculated a global average export ratio of 0.06 ± 0.03, with the SO (defined

as south of 45°S) having the lowest export ratio ($CaCO_3$:C_{org}~0.01, where C_{org} is equivalent to sinking POC). Measurements of PIC:POC across the GCB would help assess these model findings.

The importance of a ballast effect on atmospheric CO_2 is less clear. Observed correlations between deep (>2000 m) PIC flux and the absolute and relative flux of deep POC have led to hypotheses about the role of PIC in ballasting POC export [*Francois et al*., 2002; *Klaas and Archer*, 2002]. Increasing both the magnitude of POC flux to depth [*Volk and Hoffert*, 1985] and its remineralization length scale [*Kwon et al*., 2009] should lower ocean (and ultimately atmospheric) CO_2. Model studies have shown that atmospheric CO_2 is sensitive to modest changes in remineralization length scales, such that a 24 m increase in the depth at which 63% of sinking carbon is remineralized led to a decrease in atmospheric CO_2 of 10–27 ppm [*Kwon et al*., 2009].

In this work, we provide ship and satellite comparisons of PIC in the Atlantic and Indian sectors of the SO, comparing them to other data sampled globally to demonstrate the validity of the PIC algorithm for defining the GCB. We use satellite and ship data to show the large-scale pattern of coccolithophores in the GCB and discuss the effects of macronutrient and iron control on the presence of the feature. We describe an index (residual nitrate potential growth (RNPG)) that scales the excess of nitrate versus silicate to the potential growth of phytoplankton, as trace metal limitation is relieved. We then examine the effect of GCB coccolithophores on the CO_2 source/sink balance of the GCB waters and the sinking flux of POC, and we contrast this with regions containing abundant diatoms. Finally, we synthesize these points into a conceptual view on the regulation of GCB growth as well as its biogeochemical significance.

2. Methods

This study was done on research cruises between the Patagonian Shelf and Cape Town, South Africa (January–February 2011; R/V *Melville* no. 1101), and between Durban, South Africa, and Fremantle, Australia (February–March 2012; R/V *Revelle* no. 1202). Underway measurements were made for temperature, salinity, partial pressure of CO_2 (pCO_2), total particulate, and PIC-specific backscattering. Discrete measurements were made for chlorophyll, PIC, POC, biogenic silica (BSi), coccolithophore concentration, calcification, and photosynthesis. Measurements were also made of the seawater CO_2-carbonate system (i.e., dissolved inorganic carbon (DIC) and total alkalinity (TA)), iron limitation of phytoplankton (via deck experiments), and ^{234}Th-based vertical flux rates. Each of these measurements is described in detail below.

2.1. Underway and Discrete Sampling

A semicontinuous underway sampling system was used to measure hydrographic and bio-optical properties of surface seawater [*Balch et al*., 2010]. The system measured temperature, salinity, pH, and chlorophyll fluorescence. Total backscattering at 532 nm ($b_{b\ tot}$) was measured using a WetLABS ECO-VSF (three angles). Backscattering also was iteratively measured following acidification of seawater with glacial acetic acid, dropping the pH below the pK_1 for dissolution of calcite and the more soluble aragonite [*Millero*, 1996] ($b_{b\ acid}$), and by difference, acid labile backscattering ($b_{b\ tot} - b_{b\ acid} = b_b'$) [*Balch and Drapeau*, 2004], which was calibrated to PIC concentration. About every 3 h, underway, discrete water samples were collected for chlorophyll *a* [*Joint Global Ocean Flux Study*, 1996], PIC, and POC [*Poulton et al*., 2006] to calibrate the underway sensor system. Biogenic silica also was sampled using the technique of *Brzezinski and Nelson* [1989].

2.2. Satellite Data Processing for PIC

Regional PIC concentrations (mol m^{-3}) were estimated by satellite using the merged two-band/three-band algorithm [*Balch et al*., 2005; *Gordon et al*., 2001] with Moderate Resolution Imaging Spectroradiometer (MODIS)-Aqua data. The performance of the algorithm in the GCB was assessed by comparing the satellite-derived PIC concentration (mol m^{-3}) to the shipboard-derived PIC concentration (same units, estimated by multiplying the ship-measured acid-labile backscattering (b_b'; units of m^{-1}), by the average coccolithophore backscattering cross section of PIC, currently used in the NASA PIC algorithm (1.628 m^2 mol^{-1})). This algorithm comparison was made with the data taken in the cruises described here and compared to other global cruises, in which these measurements have been made previously (see Results section). Satellite-derived current velocities were estimated using satellite altimetry from the Jason-2 mission (Ocean Surface Current Analyses–Real Time (OSCAR); http://www.oscar.noaa.gov/index.html). Current velocities and directions were downloaded with 1° × 1° resolution between 30°S and 65°S around the entire SO for January 2012, for

comparison to MODIS-Aqua-derived PIC patterns from the same time period, averaged at the same time and space resolutions.

2.3. Microscopy

Total coccolith and coccolithophore abundances were measured by the HA filter/optical-adhesive technique [*Poulton et al*., 2010] with polarized light microscopy and image analysis [*Balch and Utgoff*, 2009; *Balch et al*., 2011]. Discrete water samples were run through a FlowCAM imaging cytometer for measuring particle backscattering, chlorophyll, phycoerythrin fluorescence, and imaging of nanoplankton and microplankton (4–100 μm). Particle volume was converted to cellular C according to *Menden-Deuer and Lessard* [2000].

2.4. Calcification/Photosynthesis

Water was sampled at six depths per station, and the microdiffusion technique [*Balch et al*., 2000; *Paasche and Brubak*, 1994] was used with simulated in situ, 24 h incubations in deck incubators cooled with ambient surface seawater (Atlantic sector cruise) and a deckboard heater/chiller unit (Indian sector cruise) to estimate net coccolithophore calcification (NCC) and net community organic production. Samples were filtered through 0.4 μm polycarbonate filters, rinsed, and prepared for microdiffusion analysis [*Balch et al*., 2000].

2.5. Seawater CO_2-Carbonate System Analyses at Sea

Analytical methods followed standardized protocols [*Bates et al*., 1996b, 2001; *Dickson et al*., 2007; *Knap et al*., 1993]. Both DIC and TA samples were sampled shipboard with replicate samples analyzed ashore for QC/QA purposes. TA was determined using a Versatile Instrument for Detection of TA (VINDTA) analytical system (2011 cruise) and Automated Infrared Inorganic Carbon Analyzer (AIRICA). A 25 mL or 10 mL sample volume was used for analysis of DIC analyzer samples on the VINDTA and AIRICA, respectively. Samples were also analyzed ashore using a highly precise (0.02%; 0.4 μmol kg^{-1}) VINDTA system [*Bates*, 2007; *Bates and Peters*, 2007; *Bates et al*., 1996b]. Both DIC and TA analyses had a precision and accuracy of ~1 μmol kg^{-1} (precision estimates were determined from 300 between-bottle and within-bottle replicates and accuracy assessed using calibrated reference materials for shipboard and lab work from A. Dickson, Scripps Institution of Oceanography, La Jolla, CA). Normalized alkalinity (nTA) is defined as the total alkalinity normalized to a salinity of 35. The ships were outfitted with a flow-through "SAMI" pCO_2 sensor (Sunburst Sensors) based on colorimetric methods (http://www.sunburstsensors.com/products/oceanographic-carbon-dioxide-sensor.html). Carbonic acid dissociation constants were appropriate for temperate/polar seas, and temperature, salinity, and depth data were used to compute inorganic carbon parameters (i.e., pCO_2; note that pH, $[CO_3^{2-}]$, and Ω for aragonite/calcite were not used directly in the paper) using the software, CO2calc [*Robbins et al*., 2010].

2.6. Export Fluxes of POC, PIC, and BSi

We used the ^{238}U-^{234}Th disequilibrium technique coupled with measurements of size-fractionated ^{234}Th, POC, PIC, and BSi to determine ^{234}Th-based export fluxes of POC, PIC, and BSi. Samples for ^{234}Th and size-fractionated particles were collected at a subset of stations (Figure 10c). Total ^{234}Th activity profiles were measured using the small-volume technique [*Pike et al*., 2005]. ^{234}Th export flux from the base of the euphotic zone ("z_{PAR}"), defined as the depth of the 0.3% light level, and 100 m below that ("$z_{PAR+100}$") were determined by integrating the ^{234}Th activity deficit to those depths. Note that the 0.3% light level was used here because the control of the light levels in our shipboard incubators with neutral-density screen could only be achieved to 0.3%, instead of the more typical definitions of the euphotic zone between the 1% and 0.1% light depths [*Marra et al*., 2014]. ^{234}Th fluxes were converted to POC, PIC, and BSi fluxes using measured ratios of those components to ^{234}Th in >51 μm particles collected by dual-flow, in situ filtration at z_{PAR} and $z_{PAR+100}$ [*Rosengard et al*., 2015; *Thomalla et al*., 2008]. The PIC:POC export ratio was determined from the PIC:POC ratio of >51 μm particles at z_{PAR}. A dual-flow version of battery-operated pumps by McLane Research, Inc. was used to allow simultaneous collection of particles on precombusted quartz fiber filters (for PIC, POC, and ^{234}Th) and on polyethersulfone filters (for BSi) [*Cutter et al*., 2010; *Lam et al*., 2012; *Ohnemus and Lam*, 2014; *Owens et al*., 2015]. Total and particulate ^{234}Th activities were counted using low-level Risø beta counters at sea and again after six half-lives on land. Full methodological details are reported in *Rosengard et al.* [2015].

2.7. Calculation of Residual Nitrate Potential Growth

The calculation of residual nitrate potential growth (RNPG) involves recasting the observed nitrate and silicate concentrations into potential algal growth rates, then subtracting the silicate-dependent growth rate

from the nitrate-dependent growth rate, the sign of which determines which algal groups would dominate if relieved from trace metal limitation. If the difference is positive, then this implies that potential nitrate-dependent growth will exceed silicate-dependent growth, should trace-metal limitation be removed. A negative difference implies that potential silicate-dependent (diatom) growth exceeds nitrate-dependent growth as trace metal limitation is relieved. The basic Michaelis-Menten formulation was used to describe nutrient uptake [*Caperon*, 1967; *Dugdale*, 1967].

The similarity of half-saturation coefficients for nutrient uptake and growth was noted previously [*Eppley and Thomas*, 1969], which then allowed potential growth rates to be calculated for nutrient-limited algae as shown in equation (1).

$$\mu = \mu_{\max} (S/(K_s + S)) \quad (1)$$

where μ and $\mu_{\max}$ are the specific growth rate and maximum growth rate (both units d^{-1}), respectively; S is the substrate concentration (μM); and K_s is the half-saturation constant for growth (similar to that of uptake; units of μM). Nonetheless, it is well known that species vary in their values of K_s, but in a comparison of the range of K_s values for nitrate uptake by diatoms, dinoflagellates, prymnesiophytes, and chlorophytes, the average K_s for 13 species, with 27 individual determinations, was ~1.77 μM (SE = ±0.46 μM) [*Eppley and Thomas*, 1969; *Eppley et al*., 1969]. The best known estimates of the variability of maximum growth rate of phytoplankton were made as a function of temperature [*Bissinger et al*., 2008; *Eppley*, 1972]. In this case, maximum growth rates within the 0–25°C range varied from 1 to 3 d^{-1} for nearly 200 different measurements. A more recent appraisal of 1500 different published estimates of $\mu_{\max}$ showed a similar shaped curve but with a slightly larger variability of 1–4 d^{-1} [*Bissinger et al*., 2008]. *Balch and Byrne* [1994] noted that the values of $\mu_{\max}$ and K_s were a function of the degree of eutrophy of the environments that the phytoplankton were sampled in, and they used the following simple empirical approximations to predict both parameters:

$$K_{s\,N} = ([NO_3]/(3 + [NO_3])) \times 5.5 \quad (2)$$

$$\mu_{\max\ N} = ([NO_3]/(2 + [NO_3])) \times 3 \quad (3)$$

The subscript, *N*, in equations (2) and (3) denotes the nitrate-related growth kinetics. It can be seen that in the growth rate prediction of equation (3), the maximal growth rates would asymptote at ~3 d^{-1}. Silicate uptake by diatoms differs from phytoplankton nitrate uptake; in that, diatoms typically cannot completely deplete all the silicate. The residual silicate substrate concentration, S_o, averages about 0.7 μM and was integrated into the Michaelis-Menten equation [*Paasche*, 1973a, 1973b] to predict silicate-dependent growth using equation (4).

$$\mu_{Si} = \mu_{maxSi} ((S - S_o)/(K_{s\_Si} + (S - S_o)) \quad (4)$$

where the subscript Si denotes the silicate-specific process. In the absence of comparative data on nitrate and silicate uptake kinetics across a wide spectrum of phytoplankton groups, we here assume that physiological kinetic response to variable substrate concentration will be similar for limiting nutrients, in order to maintain balanced growth [*Parslow et al*., 1984; *Shuter*, 1979]. We therefore used the same formulation given in equations (2) and (3) to approximate silicate growth kinetics, but we included S_o, in the formulation, the minimal reactive silicate concentration below which diatoms cannot utilize the nutrient (equation (4)) as observed previously by *Paasche* [1973b].

As a cross-check on the S_o assumption, we examined the number frequency of silicate concentrations measured in our Southern Ocean cruises and found that the most common silicate concentration below 5 μM was 0.5–1 μM (7.7% of the 1495 samples), while only 1.1% of the data were a true 0 μM (data not shown). This is entirely consistent with Paasche's supposition of S_o of 0.7 μM. RNPG was then calculated as

$$\text{RNPG} = \mu_N - \mu_{Si} \quad (5)$$

2.8. Assessment of Iron Limitation

Eight metal incubation experiments were performed along and around the GCB to assess potential for Fe to limit the growth of coccolithophores, diatoms, and other phytoplankton taxa. Mixed-layer water was collected from 20 m with a 30 L GO-FLO bottle deployed on Kevlar line. Bottles were immediately transported into a positive-pressure trace metal clean van, and water was dispensed gently into 10 L low-density polyethylene cubitainers. A 200 μm mesh was placed in-line to remove mesozooplankton grazers. All bottles and plastic ware were stringently acid cleaned prior to use, and trace metal clean techniques

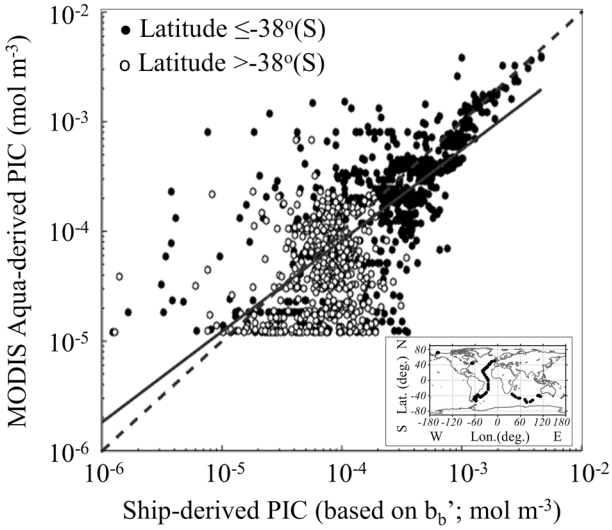

Figure 1. Validation of MODIS-Aqua-derived, merged two-band/three-band PIC algorithm [*Balch et al.*, 2005; *Gordon et al.*, 2001] (only designed for case I waters, where phytoplankton dominate the optical signal [*Mobley*, 1994]). Dashed line is the 1:1 line. Solid line is the least squares fit. Note that the logarithmic axes allow the performance of the algorithm to be assessed over ~3 orders of magnitude of PIC concentration. The least squares fit to the data (95% CI in square brackets) is $\log(Y) = 0.837\ [\pm 0.037] \times \log(X) - 0.751\ [\pm 0.141]$; $r^2 = 0.575$; RMS error = ±11%. Open symbols are the matchup points from latitudes north of the 38°S parallel and closed points are for matchups from south of the 38° parallel (in the GCB). Inset in the bottom right shows the global map of the matchup database, with observations from the GCB cruises described here, plus other cruises where the same technique was applied: Patagonian Shelf COPAS'08 [*Balch et al.*, 2014b], Atlantic Meridional Transect [*Robinson et al.*, 2009], Western Arctic [*Balch et al.*, 2014a], and Gulf of Maine North Atlantic Time Series [*Balch et al.*, 2012]. Note that the Atlantic GCB cruise in 2011 was anomalously cloudy and overcast. There were no synchronous satellite-ship matchups for PIC.

[*Bruland et al.*, 1979] were employed for all steps including conducting the work in a trace metal clean van. Cubitainers and polycarbonate incubation bottles were soaked in 1% Micro detergent for several days, then rinsed copiously with ultrapure >18.2 megohm water, and soaked in 1 M reagent HCl for several more days before being rinsed again and dried before use. Cubitainers were spiked with a Fe solution produced from a traceable AAS standard diluted into 0.01 M Optima HCl. The first two incubation experiments (experiments 1 and 2) inadvertently involved Fe additions of 0.02 nM, due to a calculation error. Experiments 3 through 8 involved Fe additions of 2 nM. Treatment cubitainers were gently homogenized, and water was decanted into triplicate 2.5 L polycarbonate bottles. Bottles were filled completely (minimizing headspace) and sealed with parafilm and vinyl tape, then placed in deckboard incubators at 50% surface irradiance. For experiments 1 through 4 (Atlantic sector cruise), incubator temperature was maintained with surface water circulated through the ship's through-hull system. There were some situations where variations in surface temperature (as we transited north or south) changed the temperature from initial conditions at which the phytoplankton community was collected. For experiments 5 through 8 (Indian sector cruise), a deckboard heater/chiller unit was used to control the temperature of recirculating seawater as the ship transited through oceanographic regions with different temperatures. The responses of phytoplankton to added Fe were assessed through measurements of total chlorophyll, biogenic Si, and PIC at the end of the incubation. Incubation experiments lasted between 3 and 6 days.

3. Results

3.1. Spatiotemporal Satellite Determination of PIC

The accuracy of the MODIS-Aqua estimates of PIC concentrations was assessed using cruise data, collected from the world ocean since 2002, the year of the launch of MODIS-Aqua (see inset to Figure 1). Satellite-derived PIC was compared to shipboard measurements of acid-labile backscattering (b_b'; units m^{-1}) that were converted to equivalent PIC concentration using the average PIC backscattering cross section ($1.628\ m^2\ (mol\ PIC)^{-1}$; value currently implemented in the official NASA PIC algorithm). The matchups (which include data from the Southern Ocean) are shown in Figure 1. The results show an RMS error of ±11% for the algorithm globally.

The highest PIC concentrations in the algorithm comparison were found south of 38°S in the GCB (Figure 1). Moreover, satellite-derived PIC and shipboard measurements of acid-labile backscattering showed highest concentrations within the Atlantic sector of the SO, decreasing eastward into the Indian sector of the GCB (Figures 2a–2c). Diversity of coccolithophore populations increased to the east: scanning electron microscope and light microscopy showed that the number of coccolithophore species increased from 1 (*E. huxleyi*) off Patagonia to 8 off Africa and 13 SW of Australia [*Smith*, 2014]. In both Atlantic and Indian sectors, PIC and

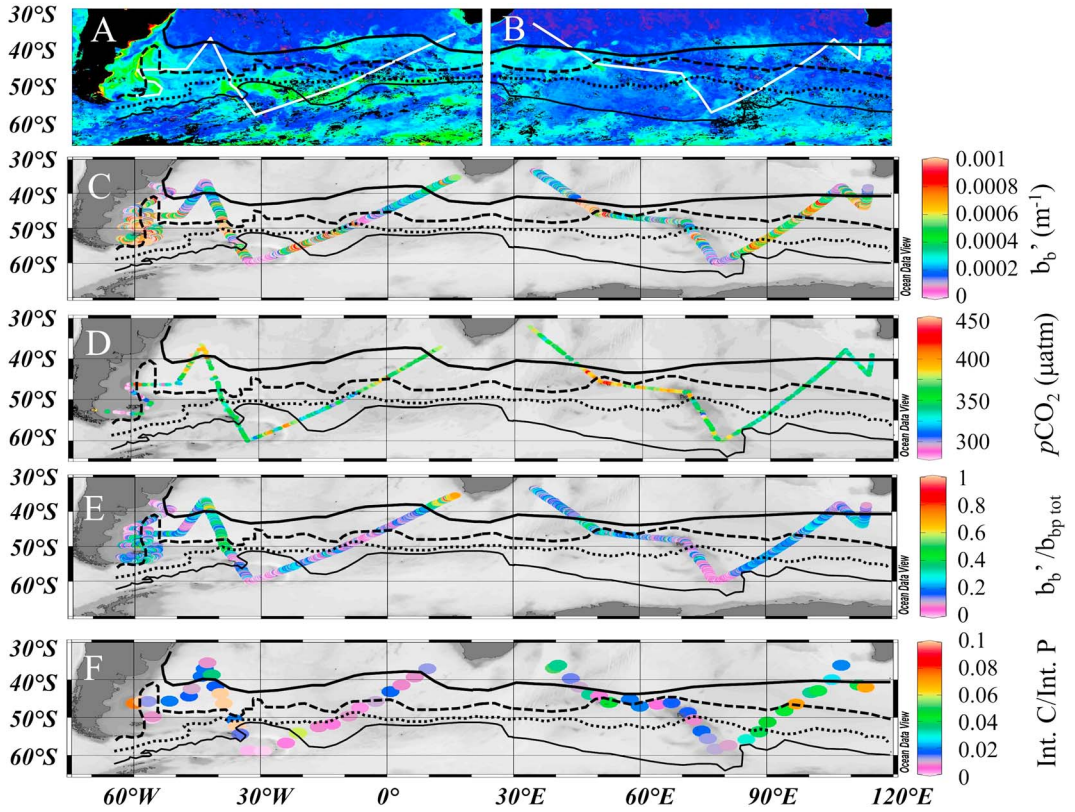

Figure 2. Geographic distribution of surface properties. (a) Cruise track of *Melville* no. 1101 overlaid on the monthly MODIS-Aqua PIC product for January 2011 (9 km binned; mol m^{-3}). (b) Cruise track of *Revelle* no. 1202 overlaid on average satellite-derived PIC for February 2012 (same spatial bins as in Figure 2a). (c) Acid-labile backscattering (backscattering from $CaCO_3$) of surface mixed layer for both GCB cruises, as well as COPAS'08 cruise over the Patagonian Shelf [*Balch et al.*, 2014b]. (d) Regions with $pCO_2 > 390$ µatm (ochre to red colors) represent a source of CO_2 to the atmosphere. Anything ≤390 µatm (ochre to indigo) represents a CO_2 sink. (e) Fraction of total backscattering contributed by PIC. (f) Integrated calcification/integrated photosynthesis measured using microdiffusion technique. For all plots, the climatological positions of the frontal boundaries are indicated with various black lines: heavy solid = Subtropical Front, medium dash = Subantarctic Front, fine dash = Polar Front, thin solid = ACC boundary [*Orsi et al.*, 1995].

coccolithophore concentrations were generally, but not always, elevated near the climatological and actual positions of the STF, SAF, PF, and the Antarctic Circumpolar Current (ACC) front (Figures 2a–2c; see overlaid density isopleths in Figure 3 for actual locations of fronts). RNPG was highest between the STF and SAF frontal regions and north of the PF. It was lowest south of the PF and in ACC waters (Figure 3a). Diatom concentration was highest inshore of the shelf front on the Patagonian Shelf, in PF and SAF waters in the Atlantic sector of the SO, and PF and ACC waters of the Indian sector SO. Lowest diatom concentrations were observed north of the STF (Figure 3b). Diatom abundance was not exclusively low in regions of positive RNPG. There were a few regions (section B and the northernmost part of section F) where there were both elevated diatoms and coccolithophores in a region of positive RNPG. However, south of the PF in both Atlantic and Indian sectors, regions of negative RNPG were characterized by a stronger diatom (than coccolithophore) response.

Satellite-derived PIC and shipboard measurements of coccolithophore concentration showed highest values within the fast-moving waters of the ACC (Figure 4), in moderate salinity Atlantic sector waters, decreasing eastward into the Indian sectors of the GCB (Figures 3c and 4). The regression between altimetry-based water velocity and PIC concentration is given in Figure 4b. There was a highly significant relationship between the binned current velocity (m s^{-1}) and binned PIC concentration (mol m^{-3}; Figure 4) (Y [±0.078] = 6.93×10^{-4} [$\pm 2.8 \times 10^{-5}$] $X^{0.202\ [\pm 0.0175]}$; $r^2 = 0.759$; $p < 0.001$).

3.2. Spatial Variability of RNPG and Coccolithophore Abundance

To assess the potential for relative growth of diatoms versus nonsilicifying phytoplankton, we examined the potential for growth (RNPG) on nitrate versus silicate in the absence of trace metal limitation. RNPG was

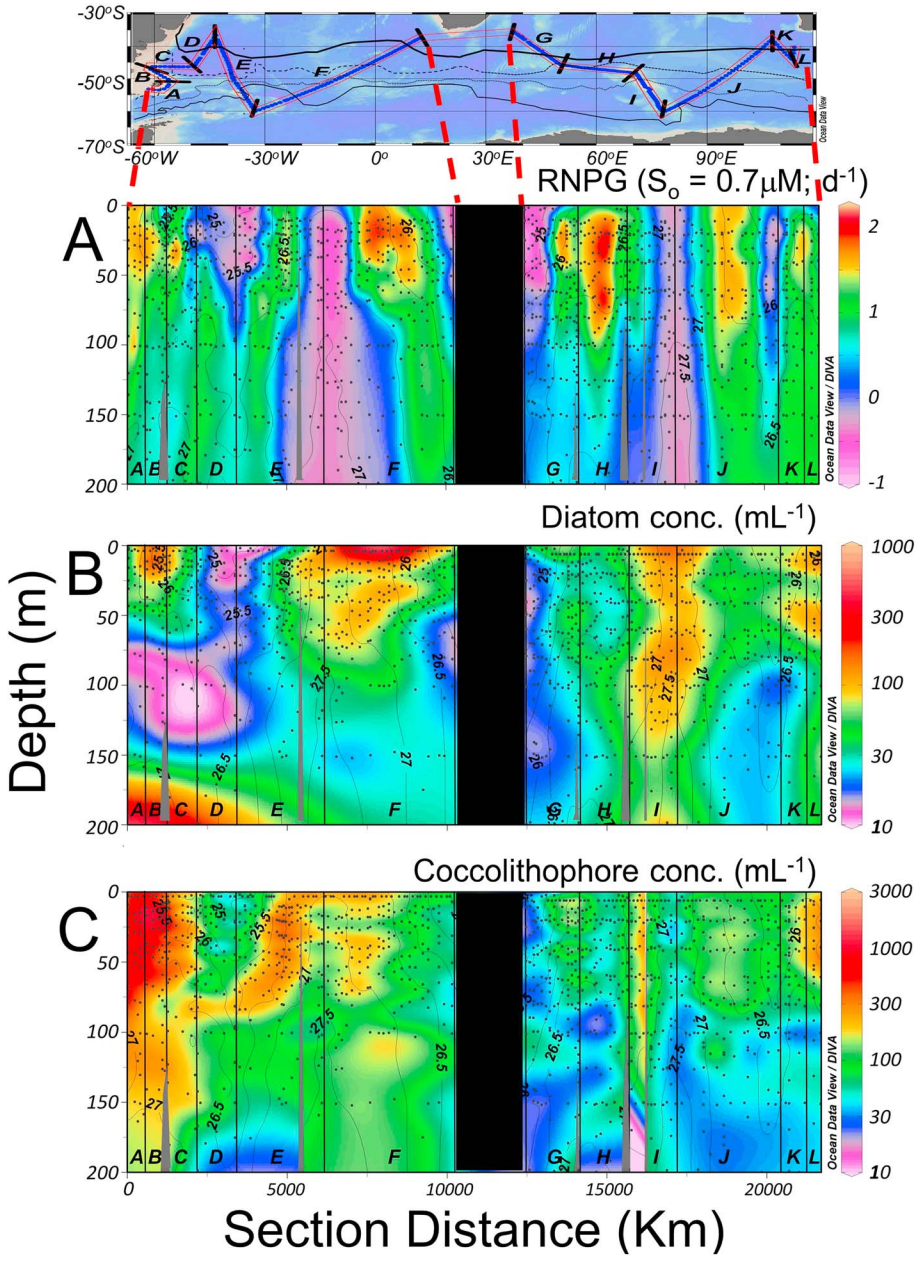

Figure 3. Vertical sections from *Melville* no. 1101 and *Revelle* no. 1202 cruises. The top inset shows the cruise track with letters designating sections of the cruise track. (a) Sections of RNPG (d^{-1}) where positive values are regions where nonsiliceous phytoplankton growth would be expected to be favored, while negative values represent regions and depths where potential diatom growth would be expected. (b) Diatom abundance (mL^{-1}) as determined with the FlowCAM. (c) Sections of coccolithophore concentration (mL^{-1}) as determined with polarized light microscopy. In all plots, vertical lines and letters designate the sections shown in inset. Frontal climatologies are indicated in top inset with different line patterns (from north to south): thick solid line = Subtropical Front, dashed line = Subantarctic Front, fine dash = Polar Front, thin solid line = ACC boundary [*Orsi et al.*, 1995]. Density isopleths overlaid onto Figures 3a–3c.

greatest in waters with temperatures of 5 to 7°C (SAF) and 10 to 12°C (STF). RNPG values were lowest south of the PF and north of the STF (Figures 3a, 5a, and 10b). Coccolith backscattering (b_b'; also called acid-labile backscattering [*Balch et al.*, 2001]; only measured along track in surface waters) increased with RNPG (Figure 5b). Coccolithophore concentration within the euphotic zone was highest in areas of positive RNPG, but silicifiers exceeded calcifiers (low PIC:BSi ratios) when RNPG was negative (Figures 3a, 3c, and 5c). In contrast, negative RNPG occurred north of the STF (where reduced nitrate concentrations limited diatom growth

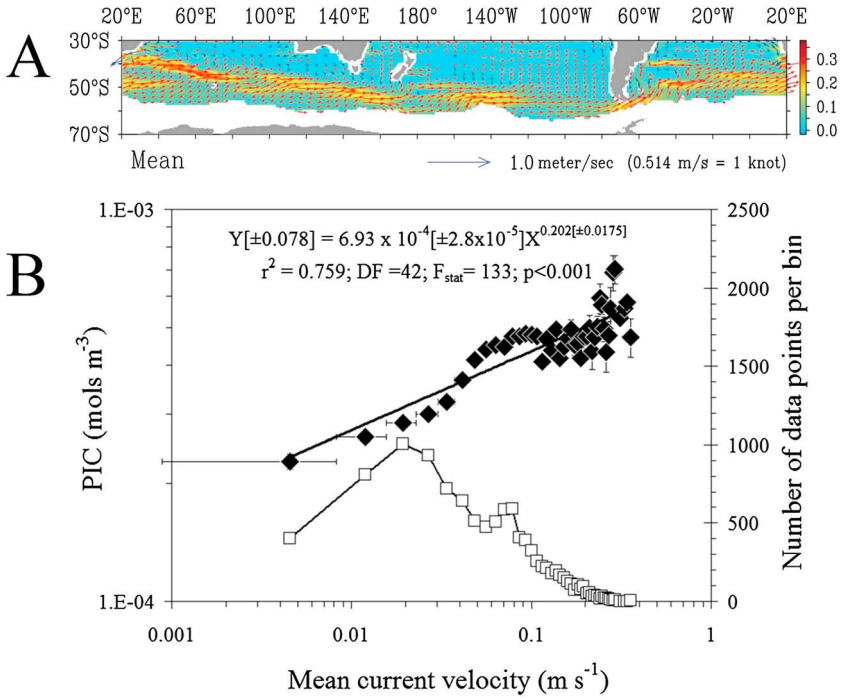

Figure 4. (a) Altimetry-based currents of Southern Ocean (from OSCAR program) color coded to velocity (scale bar on the right). (b) Average PIC concentration from MODIS-Aqua plotted against altimetry-derived current velocity (black diamonds, left *y* axis). Numbers of data points in each binned average shown as open squares (right *y* axis). Data show that highest PIC concentration is associated with fastest currents (which lie along frontal boundaries). Least squares power fit to the data also is shown.

more than growth of nonsilicious phytoplankton) and south of the PF waters (where high silicate allowed more diatom growth relative to calcifiers; Figures 5a and 5c). As shown in Figure 3, diatoms cooccurred with coccolithophores near the STF off Australia (near sections K and L) and in the SE Atlantic (along section F) but were most abundant south of the PF (Figure 3b; between sections I and J), where silicate-rich water reached the surface and RNPG was zero or negative, with diatoms increasing relative to coccolithophores (Figure 3c).

3.3. Spatial Variability of Seawater pCO_2

Seawater pCO_2 was highly variable in SAF waters, ranging from <300 to >420 μatm (Figure 2d). Large regions of the SAF zone (e.g., near the Falklands, Crozet, Kerguelen, and Heard Islands—with elevated coccolithophore biomass during January and February) had pCO_2 values up to 100 μatm higher when compared to adjacent low coccolithophore biomass areas in regions of similar temperature in the SAF. Near the Crozet Islands, a multiple linear regression of nTA as a function of b_b' and pCO_2 showed a moderate correlation ($r^2 = 0.52$; $p < 0.01$; Figure 6a). In this same region, the fraction of backscattered light contributed by PIC (b_b'/b_{bptot}, i.e., PIC:POC; Figure 2e) was accompanied by elevated surface seawater pCO_2 in a number of cases (Figure 2d). These areas also coincided with low-salinity normalized TA values and TA:DIC ratios, suggestive of alkalinity uptake due to calcification (temperature effects on pCO_2 are minimal and do not contribute to this contrast). These biogeochemical and optical features were also pronounced near the Falklands (Figure 6b) and Kerguelen (not shown here) in the SAF. Superimposing the pCO_2 concentrations over the 12 year climatological PIC concentrations generally showed highest pCO_2 concentrations in regions with historically elevated PIC concentrations (Figure 7b). Moreover, the boundaries of the elevated PIC regions near Crozet corresponded to the streamlines of current velocity [*Pollard et al.*, 2007b]. The regions of highest surface seawater pCO_2 observed during the Great Belt cruise are also co-located with regions of higher pCO_2 collected in January and February from 2010 to 2015. In Figure 7b, gridded Southern Ocean CO_2 Atlas (SOCAT) data set (version 3 [*Bakker et al.*, 2014; *Pfeil et al.*, 2013]) corresponds to mean pCO_2 in each 1° × 1° box using higher-frequency surface pCO_2 collected from the R/V *Marion Dufresne* by N. Metzl (partial data reported elsewhere [*Lourantou and Metzl*, 2011]). Figure 7b shows that limited pCO_2 data have been collected in the region over the past 6 years since 2010.

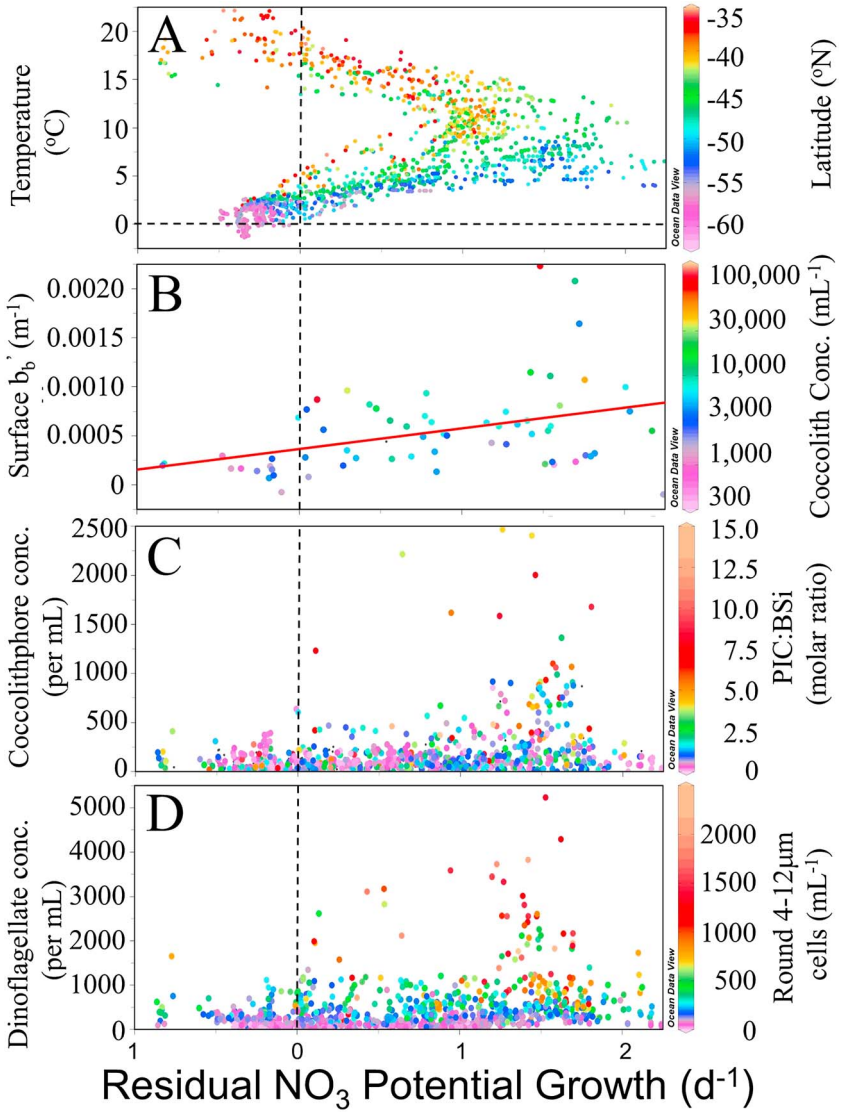

Figure 5. Residual nitrate potential growth (RNPG) plotted versus (a) temperature (*y* axis) and latitude (color of points); (b) surface acid-labile backscattering, b_b' (*y* axis; least squares linear fit to the data: $b_{bp} = 2.108 \times 10^{-4} \times \mathrm{RNPG} + 3.661 \times 10^{-4}$; $r = 0.386$; $n = 65$; $\mathrm{RMSE} = 4.005 \times 10^{-4}$) and coccolith concentration (color of data points); (c) coccolithophore concentration (per mL) and PIC:BSi molar ratio (color of points); and (d) dinoflagellate abundance and concentration of 4–12 µm diameter nanophytoplankton (color of data points). Data from Figures 5a, 5c, and 5d are from multiple depths, while data from Figure 4b were collected from the surface only.

3.4. Iron Limitation of Phytoplankton Community, Including Coccolithophores and Diatoms

Incubation experiments showed significant ($p < 0.05$, one-tailed *t* test) responses of phytoplankton to added Fe mostly in the Indian sector of the GCB, with generally negligible responses in the Atlantic sector (Figure 8). Experiment 1 (closest to Patagonian shelf) showed a small (6 ± 3% enhancement over the control) but significant enhancement of Chl in response to added Fe. The remaining three Atlantic experiments did not show significant Chl responses. Accumulation of BSi and PIC were not stimulated, relative to controls, in any of the Atlantic experiments. In the Indian sector, Fe stimulated significant Chl accumulation over the unamended controls in each of the experiments conducted south of subtropical waters (which had a starting nitrate concentration of just 0.1 µM). The addition of Fe also stimulated growth of coccolithophores (assessed via accumulation of PIC) in the Indian sector of the GCB. PIC responded significantly to Fe in experiment 6 (in between Crozet and Kerguelen Islands) and experiment 8 (southwest of Australia). Furthermore, in both of these experiments control-normalized response of PIC was approximately 45% greater than the response

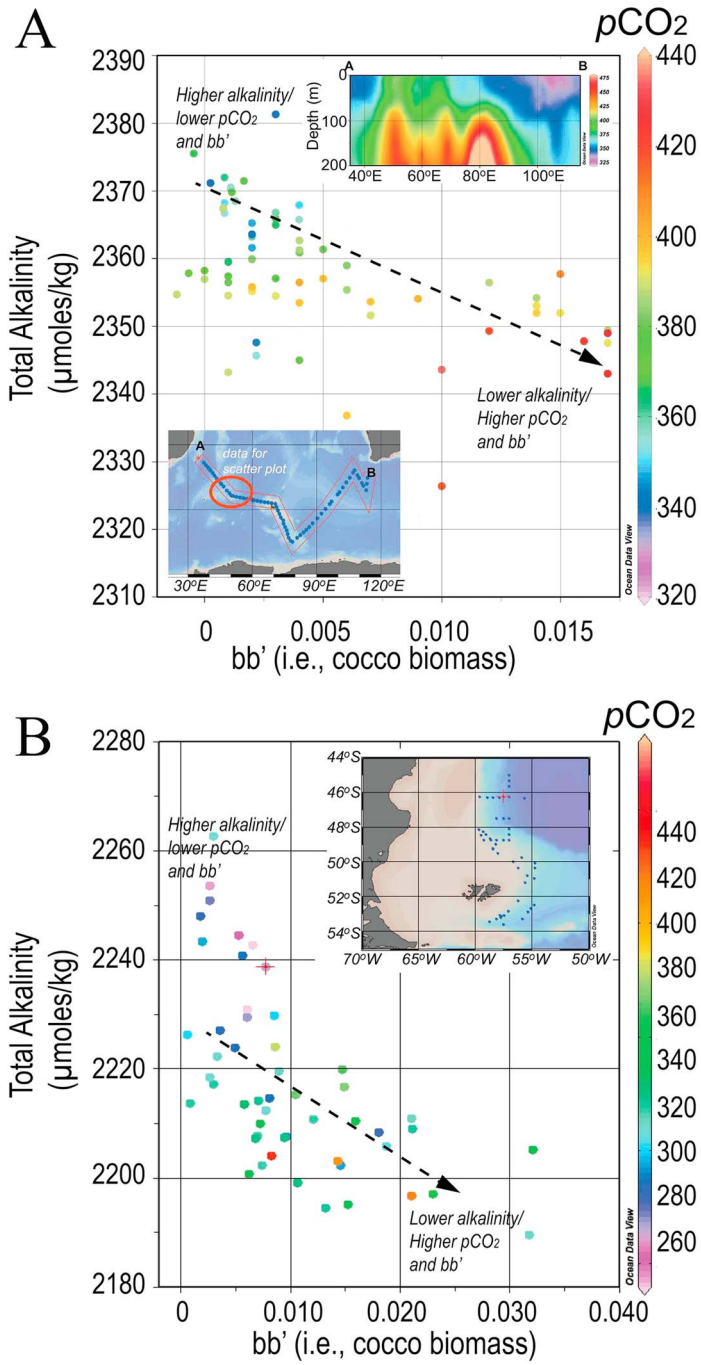

Figure 6. (a) Salinity-normalized total alkalinity versus acid-labile backscattering (b_b') from region near Crozet Islands (circled in inset at bottom) and (b) in deep water offshore of the Patagonia shelf in the South Atlantic Ocean. In Figure 6 a (data from cruise RR1202), the top inset shows the seawater pCO_2 (color scale goes from 325 to 475 ppm), where A and B mark the start and end of the transect (also shown in bottom inset map). This inset illustrates that the surface pCO_2 features extend through the mixed layer. Multiple linear regression between nTA (independent variable) and b_b' and pCO_2 (dependent variables) is shown with dashed black line: nTA [±6.678] = 2432.527 [±17.369] − 6650.91 [±2047.77] (b_b') − 0.18785 [±0.04736] × pCO_2. (Numbers in square brackets are the SE of each fit term.) Other statistics for multiple linear regression: $r^2 = 0.529$; degrees of freedom = 62; $p < 0.01$. In Figure 6b (including data from cruise MV1101 as well as COPAS'08 (Knox 22RR)) [*Balch et al.*, 2014b], the top inset shows the locations of underway and CTD-hydrocast stations for similar data as in Figure 6a but around the Patagonian Shelf region. The scatterplot for total alkalinity versus b_b' is also given, as in Figure 6a. Multiple linear regression between nTA (independent variable) and b_b' and pCO_2 (dependent variables) is shown with dashed black line: nTA [±12.0810] = 2279.64 [±12.8357] − 10776.85 [±2568.10] (b_b') − 0.1628 [±0.0428] × pCO_2. Other statistics for multiple linear regression: $r^2 = 0.522$; degrees of freedom = 50; $p < 0.01$.

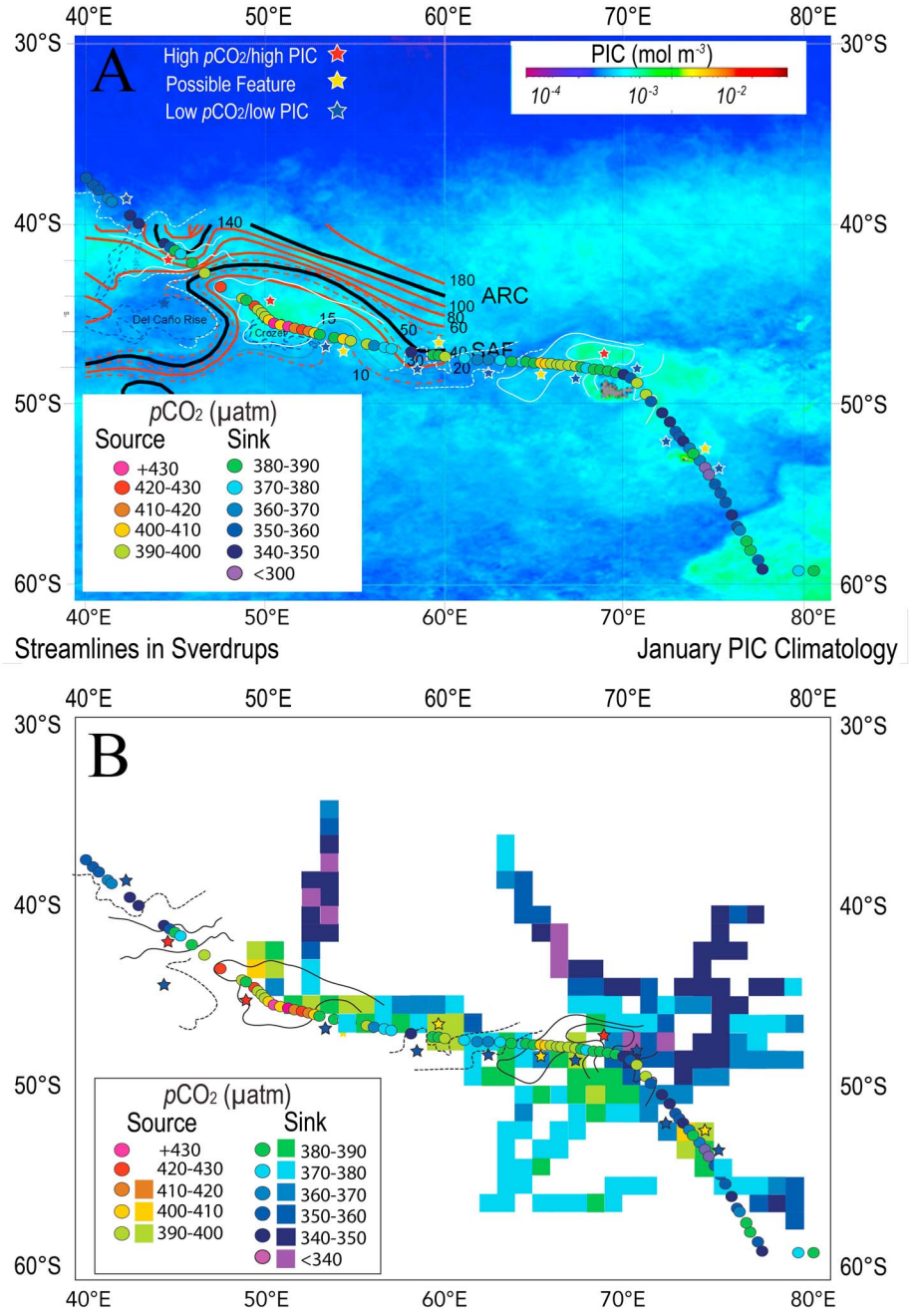

Figure 7. Results from *Revelle* no. 1202 cruise, near Crozet Islands (Indian sector of the SO) superimposed on 12 year MODIS-Aqua climatology for PIC using merged two-band, three-band PIC algorithm [*Balch et al.*, 2005; *Gordon et al.*, 2001]. (a) The color bar gives PIC concentration in mol m^{-3}, with white lines denoting approximate regions of higher PIC. Streamlines of current velocity (sverdrups = 10^6 m^3 s^{-1}) also superimposed from *Pollard et al.* [2007a] (solid black lines are 0, 40, and 140 Sv isolines; from the CROZEX experiment, 2004–2005). Solid red lines give 20 Sv increments, while dashed red lines provide further intermediate levels. ARC designates the Agulhas Return Current. Seawater pCO_2 from our cruise (circle symbols) is shown in Figure 7a along with star symbols that denote approximate locations of high PIC or low PIC features. (b) Surface pCO_2 data from the Great Belt cruise are shown against underlying, gridded (1° × 1°) surface pCO_2 data collected during the months of January and February from 2010 to 2015. These latter data represent the limited SOCAT data (version 3 [*Bakker et al.*, 2014; *Pfeil et al.*, 2013]) collected in the region. The approximate regions of higher PIC in the region are superimposed from Figure 7a. Location of Crozet Islands is also marked.

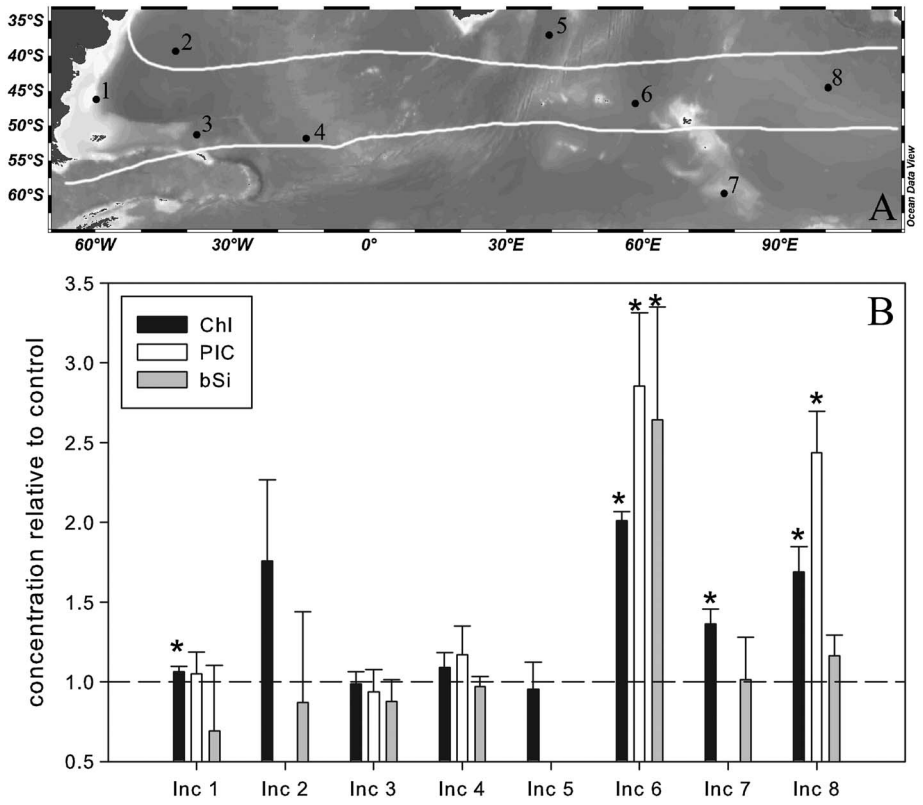

Figure 8. (a) Locations of incubation experiments. White lines represent the climatological locations of the Subtropical (northmost) and Polar (southmost) Fronts. (b) Relative response of total Chl *a*, PIC, and BSi relative to unamended control for eight different experiments, in which Fe additions were made (0.2–2 nM). Error bars represent 1 standard deviation for triplicate measurements. Asterisks indicate the values significantly greater than 1.

of total chlorophyll (Figure 8), suggesting that coccolithophores were preferentially stimulated by Fe compared to the overall phytoplankton community. In contrast, coccolithophores were not stimulated in the experiments performed in the Atlantic sector of the GCB (experiments 1, 3, and 4) nor did Fe stimulate PIC in the experiments conducted either north of the GCB (experiments 2 and 5: nitrate $<1\,\mu M$) or south of the GCB (experiment 7; ambient water 1.1°C), suggesting that something other than Fe was constraining coccolithophore growth. Biogenic silica (a proxy for diatom biomass) was significantly stimulated by Fe only in experiment 6 (in the GCB between Crozet and Kerguelen).

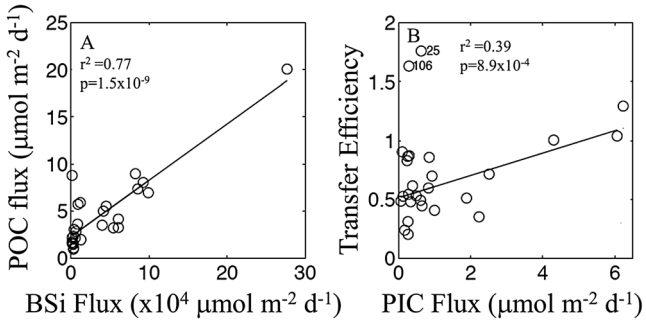

Figure 9. (a) ^{234}Th-derived POC flux as a function of BSi flux at z_{PAR}. (b) POC flux transfer efficiency between the base of the euphotic zone (z_{PAR}) and 100 m below (defined as POC flux at $z_{PAR\,+\,100\,m}$ divided by POC flux at z_{PAR}) as a function of PIC flux. Significant linear relationships are plotted as a solid black line. Transfer efficiency values at stations GB1-25 and GB2-106 were excluded from all correlations because of suspected sampling issues at those stations (figure adapted from *Rosengard et al.* [2015]).

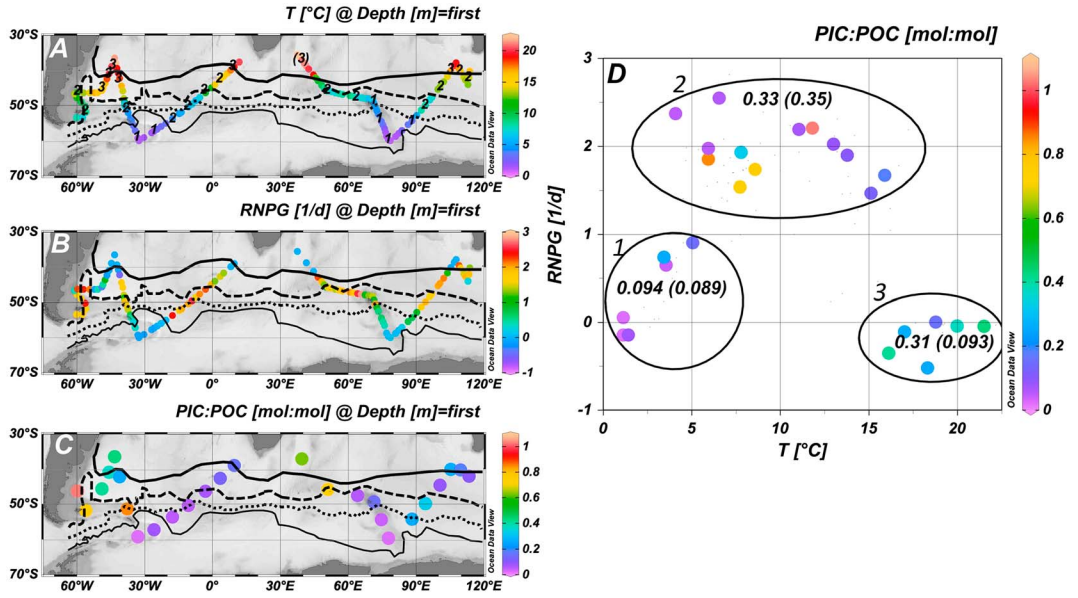

Figure 10. Relationships between temperature, RNPG, and PIC:POC. (a) Map showing sea surface temperature (numbers mark the locations of thorium flux measurements and their magnitude referring to groupings in Figure 10d), (b) map showing the surface values of residual nitrate potential growth (RNPG) along the cruise track, (c) map showing the PIC:POC export ratio at 100 m, and (d) scatterplot of RNPG versus SST (color represents the PIC:POC export ratio). PIC:POC export ratio was the ratio of PIC flux to POC flux at the base of the euphotic zone. Stations were grouped by similarities in RNPG and temperature (ovals), and the mean (1 standard deviation) PIC:POC export ratios are indicated for each group. Leftmost group is designated as the polar group (1), top middle group is the subpolar group (2), and the rightmost group is the subtropical group (3); locations and group number are indicated on the SST map in Figure 10a. Station marked in Figure 10a as "(3)" is undefined for RNPG because $NO_3 = 0$. If included in the subtropical group, PIC:POC export ratio in that group would be 0.36 ± 0.15. Climatological frontal boundaries are indicated in Figures 10a–10c as in Figure 2.

3.5. Export Fluxes

During both cruises, the ^{238}U-^{234}Th disequilibrium results showed that the magnitude of shallow POC export flux at the base of the euphotic zone (z_{PAR}~100 m) was *not* correlated with PIC export flux (not shown [*Rosengard et al.*, 2015]) but rather was correlated with BSi export flux ($r^2 = 0.74$; Figure 9a). In contrast, we found a significant correlation between the transfer efficiency of POC flux in the upper mesopelagic zone —defined as the ratio of the POC fluxes 100 m below the base of the euphotic zone (at $z_{PAR+100}$) to the POC fluxes at the base of the euphotic zone (at z_{PAR})—and the PIC export flux (Figure 9b; $r^2 = 0.39$, $p < 0.001$), but not the BSi export flux (not shown [*Rosengard et al.*, 2015]).

The minimum, median, and maximum PIC:POC export ratios (the ratio of PIC flux to POC flux at z_{PAR}) were 0.018, 0.176, and 1.03, respectively (Figure 10d). PIC:POC export ratios were grouped on the basis of observed RNPG and sea surface temperature. Polar regions (defined as RNPG < 1 and SST < 10°C) and subtropical regions (defined as RNPG < 1 and SST > 10°C) had low (0.094 ± 0.089) and high (0.31 ± 0.093) PIC:POC export ratios, respectively (Figure 10). The highest PIC:POC export ratios (>0.7) were in subpolar regions (RNPG > 1), which also had the highest mean PIC:POC export ratio but with high variability (0.33 ± 0.35; Figure 10).

4. Discussion

Our results confirm that within Atlantic and Indian sectors of the SO, satellite measurements of the GCB are matched by elevated acid-labile backscattering and coccolithophore concentrations, consistent with a coccolithophore PIC source of the elevated reflectance. This finding is also in agreement with prior coccolithophore observations in the SO [*Balch et al.*, 2014b; *Holligan et al.*, 2010; *Rembauville et al.*, 2016; *Smith*, 2014]. Furthermore, our observations showed highest (a) coccolith light scattering, (b) PIC:BSi, and (c) abundance of coccolithophores and nonsiliceous phytoplankton when RNPG was positive (Figures 3 and 5) [*Eynaud et al.*, 1999], suggesting that potential growth of nonsilicious phytoplankton was greater than growth of diatoms in these waters. This is the first observation over basin scales in the SO that PIC concentration covaries

with regions of greatest current velocity. We suggest that this occurs due to Ekman pumping along the frontal boundaries of the SO current system, and possible upwelling of iron [*de Baar et al*., 1995], which combined with the elevated nitrate relative to silicate (+RNPG) made for optimal conditions for increased abundance of nonsilicious phytoplankton (including coccolithophores) as opposed to diatoms (Figures 3 and 5). The iron incubation results demonstrate that iron can control the distribution and growth of coccolithophores in the GCB, with iron limitation of coccolithophores observed in the Indian sector of the GCB, where dust sources are most remote and ambient PIC levels are lower (Figures 2a and 2b). Iron availability may thus influence the balance between calcification (e.g., NCC) and POC production (e.g., NCP) by other phytoplankton groups, as shown by the bigger response of PIC than Chl to added Fe near Crozet, with the balance also impacting seawater pCO_2.

The seasonal occurrence of coccolithophore calcification in the GCB has a significant impact on CO_2 dynamics near the SAF. This was also seen in data from CROZet natural iron bloom and EXport experiment (CROZEX) and the Southern Ocean CO_2 Atlas (SOCAT version 3) [*Bakker et al*., 2014; *Pfeil et al*., 2013]. Deepwater TA supply to the Southern Ocean increases alkalinity tracers such as TA* [*Fry et al*., 2015] with drawdown of TA observed in the GCB co-located with regions of high seasonal coccolithophore biomass. TA* (in units of μmol kg^{-1}) is calculated as

$$TA^* = Alk_3 - 2300$$

where

$$Alk_3 = \frac{\left(Alk_m - Alk_r + \left(1.36 \times NO_3^-\right)\right)}{S} \times 35 + Alk_r$$

and Alk_m is the observed alkalinity and Alk_r is the riverine TA end-member [*Fry et al*., 2015].

Ignoring gas exchange and horizontal transport, the summer cooccurrence of high coccolithophore biomass with elevated pCO_2 (i.e., seasonal change in $pCO_2 = CO_{2SEASONAL}$) reflects the dominant influence on CO_2 due to a combination of upwelling ($\delta CO_{2UPWELLING}$), net community organic production (NCP; δCO_{2NCP}), and net community calcification (NCC; δCO_{2NCC}), such that $CO_{2SEASONAL} = \delta CO_{2UPWELLING} + \delta CO_{2NCP} + \delta CO_{2NCC}$. In areas where upwelling and Ekman pumping bring up nutrients and CO_2, seasonal organic carbon production (i.e., NCP), δCO_{2NCP}, is likely greater than $\delta CO_{2UPWELLING}$ with the net result that seawater pCO_2 decreases. However, in areas of high coccolithophore growth and biomass, generation of CO_2 by calcification offsets the drawdown of CO_2 by organic production. Thus conceptually, there are three scenarios explaining the range of seawater pCO_2 observed across the SAF waters in the GCB: (1) where NCP > NCC, seawater pCO_2 is likely to decrease; (2) where NCP~NCC, seawater pCO_2 is likely to remain unchanged; and (3) where NCP < NCC, seawater pCO_2 is likely to increase. These three scenarios all likely occur in the GCB.

In the third scenario, coccolithophore calcification in the SAF can potentially shift waters from a CO_2 sink to source (Figures 2d, 6, and 7), hinted at in a few previous studies in the Sargasso Sea, Bay of Biscay, and the North Atlantic Ocean [*Bates*, 2007; *Robertson et al*., 1994; *Smith et al*., 2012]. Recently, *Salter et al.* [2014] highlighted the importance of the carbonate counter pump (long-term production of CO_2 associated with $CaCO_3$ precipitation [*Zeebe*, 2012]) in regions of the Southern Ocean, including around Crozet. We confirm this directly for the first time with measurements of seawater pCO_2. Such shifts in the CO_2 sink-source status of SAF surface waters have direct relevance to global air-sea CO_2 fluxes and coccolithophore-CO_2 feedback.

Another diagnostic for the importance of the carbonate counter pump is the PIC:POC export ratio (rain ratio), which is an important control for atmospheric CO_2 [*Archer et al*., 2000]. Using an ocean biogeochemical-transport box model, *Sarmiento et al.* [2002] determined a global PIC:POC export ratio of 0.06, with highest values in subtropical gyres (~0.08 in the subtropical Atlantic and Indian Oceans) and lowest values in the Southern Ocean (~0.01 in the Southern Ocean Atlantic and Indian subpolar gyres, defined as waters south of 45°S). Our estimates of PIC:POC export ratio using the PIC:POC ratio of >51 μm particles were considerably higher (0.08–1.08), but the patterns we found were broadly similar, with polar and subtropical waters having consistently low and high PIC:POC export ratios, respectively (Figure 10). One notable difference was that we also found variable PIC:POC export ratios in subpolar waters. Differences in the magnitude of our estimates are likely due to the different time scales of integration represented by the two methods. The *Sarmiento*

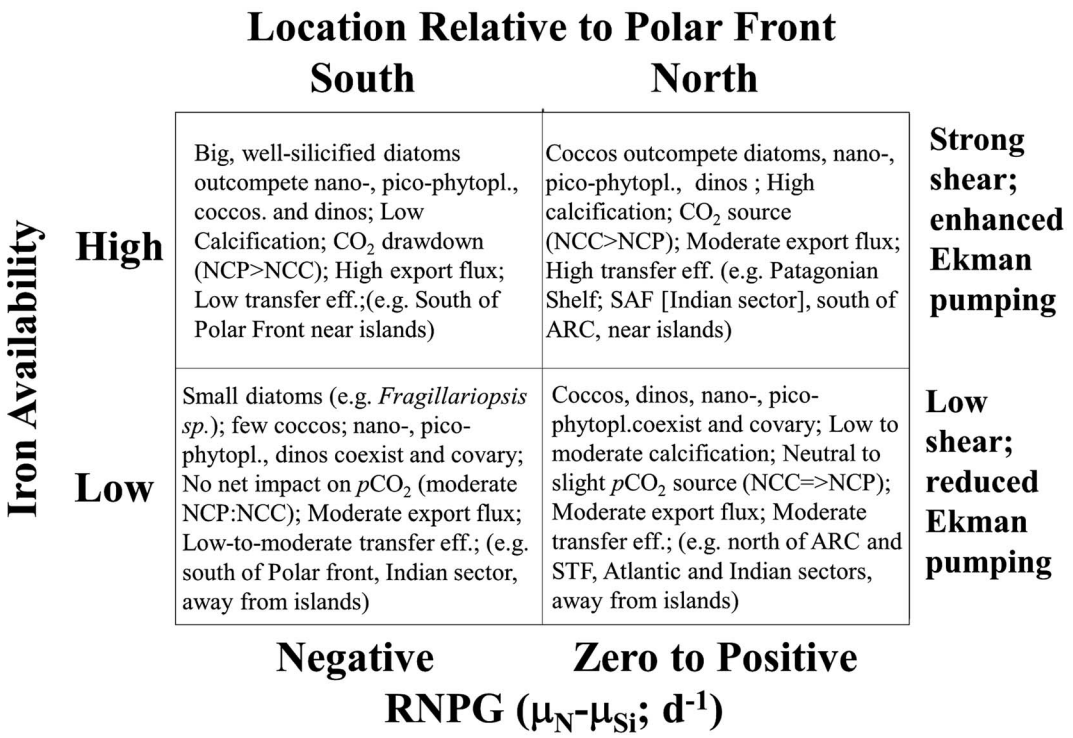

Figure 11. Conceptual model for balance of coccolithophores and noncalcifying phytoplankton growth in GCB versus diatom growth (determined as RNPG) and effects on CO_2 source/sink dynamics and sinking particle fluxes. Abbreviations used in table: coccos = coccolithophores; dinos = dinoflagellates; nanophytopl. = nanophytoplankton; picophytopl. = picophytoplankton; eff. = efficiency; ARC = Agulhas Return Current.

et al. [2002] estimate uses observed profiles of DIC, alkalinity, and NO_3, usually taken during summertime cruises, for their calculations, and represents an integration over the growing season. In contrast, our estimate is based on a snapshot of the large particle population at the time of sampling by in situ filtration. Since our cruises were timed to maximize expected coccolithophore production, our estimate may represent times of highest PIC:POC export ratio.

Time scales of integration aside, we still find that the highest PIC:POC export ratios (>0.7) were all in subpolar waters south of 45°S adjacent to the Patagonia Shelf or Crozet Island, with RNPG > 1 (Figure 10). Away from these putative trace metal sources in waters with RNPG > 1, PIC:POC export was low (Figure 10c). Export was generally not measured in fronts because of the strong current velocities and logistical difficulties in sampling in these dynamic regions. Given the high PIC detected in regions of high velocity (Figure 4), we speculate that these would also be regions of high PIC:POC export ratio. Subpolar waters with RNPG > 1 thus have very variable PIC:POC export ratios (Figure 10)—high when near a source of trace metals, and potentially in fronts, and low otherwise.

Recent global estimates of the Alk* tracer [*Fry et al.*, 2015], which isolates the effects of $CaCO_3$ cycling on alkalinity, show elevated Alk* in the Southern Ocean [*Carter et al.*, 2014; *Fry et al.*, 2015]. Elevated Alk* in the Southern Ocean is thought to result from the upwelling of high Alk* waters, and does not preclude calcification in surface waters, which would otherwise tend to decrease Alk*. Indeed, further evidence of sustained PIC production in the GCB comes from the sediment composition in the STF and SAF zones dominated by $CaCO_3$ [*Longhurst*, 1998]. Overall, evidence suggests that the STF and SAF zones have a relatively high PIC:POC export ratio, which would thus act to increase ocean CO_2.

Our ^{234}Th flux results (Figure 9) add to the growing body of evidence that there is not a universal $CaCO_3$ ballast effect operating in the upper ocean [*Le Moigne et al.*, 2012; *Riley et al.*, 2012; *Thomalla et al.*, 2008]. Instead, the correlation between PIC flux and the transfer efficiency of POC flux through the upper mesopelagic (Figure 9b) suggests a role for PIC in extending the remineralization length scale of sinking POC.

However, regions of more efficient transfer of the exported POC flux to the mesopelagic were not high POC flux regions. We suggest that the CO_2-enhancing role of the carbonate pump is more important than any ballast-induced enhancement of the soft-tissue POC pump. A corollary to this is that any reduction in calcification due to ocean acidification should be expected to have a greater impact on the carbonate pump than the soft tissue pump and thus be an overall negative feedback on pCO_2 [*Riebesell et al*., 2009].

Based on this work, we propose a conceptual model on the growth of phytoplankton in the SO. Our results can be divided into a four-way mandala (Figure 11), where RNPG primarily determines whether diatoms can outcompete nonsiliceous phytoplankton (including coccolithophores) when relieved of a limiting micronutrient (Figure 8), while iron further regulates the growth of all phytoplankton in ACC waters. Each quadrant has different biogeochemical ramifications to the seawater pCO_2 and export carbon fluxes.

4.1. Synthesis and Conclusions

A synthesis of our previous data and other studies demonstrates the following consistencies in our understanding of the GCB and its biogeochemical significance to the SO:

1. The GCB is *indeed* a globally substantial feature that occurs seasonally across the STF/SAF zones and has elevated concentrations of coccolithophores relative to other regions and elevated PIC:POC export ratios.
2. In the PIC-rich waters of the GCB, calculated seawater pCO_2 is elevated in comparison to adjacent waters with lower seawater pCO_2. These features are co-located with drawdown of TA and low TA:DIC ratios that, in comparison to other areas of the GCB, suggest substantial calcification.
3. Iron supply is implicated in the reduced growth of coccolithophores in the Indian sector (and likely the Pacific sector given reduced satellite-derived PIC levels there). However, the relative lack of coccolithophores to the north and south of the GCB appears to be controlled by factors other than iron availability (i.e., macronutrients or temperature).

It should be noted that the ratio of PIC to alkalinity drawdown is not uniform in the GCB, and PIC is not high enough to account for the entire alkalinity drawdown. This is likely due to the coccolithophore bloom timing and the growth of other species. The inconsistency between PIC and alkalinity is probably simply due to sinking of the PIC over the course of the season (the carbonate pump).

Our GCB observations from the Crozet region (with its strong frontal gradients in N, Si, and Fe) can be compared to the previous results of the CROZEX experiment [*Moore et al*., 2007; *Pollard et al*., 2007a] to address the bottom-up control of coccolithophores and other phytoplankton in the GCB, including the biogeochemical implications of differential limitation by nutrients. CROZEX was performed between November 2004 and mid-January 2005. These waters were shown to have variable iron content, such that water originating from the south or east of Crozet and flowing over shallow sediments had elevated iron while water from the north or west had low iron [*Planquette et al*., 2007]. The October CROZEX observations primarily followed the demise of the spring diatom/*Phaeocystis* bloom [*Pollard et al*., 2007a]. However, PIC was present in the area; between early November and early December 2004, PIC levels were 0.25–0.75 $\mu mol\,L^{-1}$, while from mid-December to mid-January, levels were 1–1.25 $\mu mol\,L^{-1}$ (as high as 1.75 $\mu mol\,L^{-1}$ in a large eddy), representative of levels found in a moderate coccolithophore bloom [*Read et al*., 2007]. MODIS imagery from early January 2005 showed that the entire SAF region north of Crozet had minimal chlorophyll, but with ~50% higher 550 nm reflectance, suggesting a large region of coccolith-rich water in the SAF, precisely what we observed in the GCB. As noted earlier, the boundaries of the elevated PIC regions near Crozet corresponded to the streamlines of current velocity [*Pollard et al*., 2007b], suggesting bottom-up forcing of PIC production associated with Ekman pumping along the current boundaries.

Strong CO_2 drawdown dominated during CROZEX early in the growing season north of Crozet [*Bakker et al*., 2007] (our scenario NCP > NCC). During the late February 2012 cruise, coccolithophores appear to have grown sufficiently long to enhance NCC:NCP and CO_2 supply. We suspect that this temporal shift from diatom to coccolithophore production is the same as observed elsewhere when silicate is exhausted [*Balch et al*., 2014b; *Boyd et al*., 2010; *Leblanc et al*., 2009], except our results suggest that iron availability can influence coccolithophore production and the seawater pCO_2 balance of the GCB. Future work should expand the regional analyses of coccolithophores and pCO_2 to other sectors of the Southern Ocean, particularly in the Australian and Pacific sectors, where few observations have been made.

Acknowledgments
Data from this study are available at the Biological and Chemical Oceanography Data Management Office (http://www.bco-dmo.org/). We gratefully acknowledge R. Schlitzer (Ocean Data View, odv.awi.de, 2015) for the Ocean Data View software used to visualize the results in Figures 2, 3, 5, 6, 8, and 10. The Surface Ocean CO_2 Atlas (SOCAT) is an international effort, endorsed by the International Ocean Carbon Coordination Project, the Surface Ocean Lower Atmosphere Study, and the Integrated Marine Biogeochemistry and Ecosystem Research program, to deliver a uniformly quality-controlled surface ocean CO_2 database. The many researchers and funding agencies responsible for the collection of data and quality control are thanked for their contributions to SOCAT. We would like to thank Nicolas Metzl (LOCEAN/IPSL/CNRS) for the kind use of pCO_2 data from the Crozet-Kerguelen region. We gratefully acknowledge reviews by Marlon Lewis (Dalhousie University, Halifax, NS) and an anonymous reviewer. National Science Foundation (OCE-0961660 to W.M.B. and B.S.T., OCE-0728582 to W.M.B., OCE-0961414 to N.R.B., and OCE-0960880 to P.J.L.) and National Aeronautical and Space Administration (NNX11AO72G, NNX11AL93G, NNX14AQ41G, NNX14AQ43A, NNX14AL92G, and NNX14AM77G to W.M.B.) supported this work.

References

Aksnes, D. L., J. K. Egge, R. Rosland, and B. R. Heimdal (1994), Representation of *Emiliania huxleyi* in phytoplankton simulation models. A first approach, *Sarsia*, *79*(4), 291–300.

Archer, D., and E. Maier-Reimer (1994), Effect of deep-sea sedimentary calcite on preservation on atmospheric CO_2 concentration, *Nature*, *367*, 260–263.

Archer, D. E., G. Eshel, A. Winguth, W. Broecker, R. Pierrehumbert, M. Tobis, and R. D. A. Jacob (2000), Atmospheric pCO_2 sensitivity to the biological pump in the ocean, *Global Biogeochem. Cycles*, *14*, 1219–1230, doi:10.1029/1999GB001216.

Bakker, D. C. E., M. C. Nielsdottir, P. J. Morris, H. J. Venables, and A. J. Watson (2007), The island mass effect and biological carbon uptake for the subantarctic Crozet Archipelago, *Deep Sea Res., Part II*, *54*, 2174–2190.

Bakker, D. C. E., et al. (2014), An update to the Surface Ocean CO_2 Atlas (SOCAT version 2), *Earth System Sci. Data*, *6*(1), 69–90.

Balch, W., and P. Utgoff (2009), Potential interactions among ocean acidification, coccolithophores and the optical properties of seawater, *Oceanography*, *22*(4), 146–159.

Balch, W. M., and C. F. Byrne (1994), Factors affecting the estimate of primary production from space, *J. Geophys. Res.*, *99*, 7555–7570, doi:10.1029/93JC03091.

Balch, W. M., and D. T. Drapeau (2004), Backscattering by coccolithophorids and coccoliths: Sample preparation, measurement and analysis protocols, in *Ocean Optics Protocols For Satellite Ocean Color Sensor Validation, Revision 5: Biogeochemical and Bio-Optical Measurements and Data Analysis Protocols*, edited by J. L. Mueller, G. S. Fargion, and C. R. McClain, pp. 27–36, Natl. Aeronaut. and Space Admin., Goddard Space Flight Space Cent., Greenbelt, Md.

Balch, W. M., D. Drapeau, and J. Fritz (2000), Monsoonal forcing of calcification in the Arabian Sea, *Deep Sea Res., Part II*, *47*, 1301–1337.

Balch, W. M., D. T. Drapeau, J. Fritz, B. Bowler, and J. Nolan (2001), Optical backscattering in the Arabian Sea—Continuous underway measurements of particulate inorganic and organic carbon, *Deep Sea Res., Part I*, *48*, 2423–2452.

Balch, W. M., H. R. Gordon, B. C. Bowler, D. T. Drapeau, and E. S. Booth (2005), Calcium carbonate budgets in the surface global ocean based on MODIS data, *J. Geophys. Res.*, *110*, C07001, doi:10.01029/02004JC002560.

Balch, W. M., D. T. Drapeau, B. C. Bowler, and E. Booth (2007), Prediction of pelagic calcification rates using satellite measurements, *Deep -Sea Res. II (Chapman Calcification Conf. Spec. Vol.)*, *54*, 478–495.

Balch, W. M., B. C. Bowler, D. T. Drapeau, A. Poulton, and P. Holligan (2010), Biominerals and the vertical flux of particulate organic carbon from the surface ocean, *Geophys. Res. Lett.*, *37*, L22605, doi:10.1029/2010GL044640.

Balch, W. M., D. T. Drapeau, B. C. Bowler, E. S. Booth, E. Lyczskowski, and D. Alley (2011), The contribution of coccolithophores to the optical and inorganic carbon budgets during the Southern Ocean Gas Experiment: New evidence in support of the "Great Calcite Belt" hypothesis, *J. Geophys. Res.*, *116*, C00F06, 1–14, doi:10.1029/2011JC006941.

Balch, W. M., D. T. Drapeau, B. C. Bowler, and T. Huntington (2012), Step-changes in the physical, chemical and biological characteristics of the Gulf of Maine, as documented by the GNATS time series, *Mar. Ecol. Progress Ser.*, *450*, 11–35.

Balch, W. M., B. C. Bowler, L. C. Lubelczyk, and M. W. Stephens (2014a), Aerial extent and composition of a massive under-ice algal bloom in the Arctic, *Deep Sea Res., Part II*, *105*, 42–58.

Balch, W. M., D. T. Drapeau, B. C. Bowler, E. Lyczskowski, L. C. Lubelczyk, S. C. Painter, and A. J. Poulton (2014b), Surface biological, chemical and optical properties of the Patagonian Shelf coccolithophore bloom, the brightest waters of the Great Calcite Belt, *Limnol. Oceanogr.*, *59*(5), 1715–1732.

Bates, N. R. (2007), Interannual variability of the oceanic CO_2 sink in the subtropical gyre of the North Atlantic Ocean over the last two decades, *J. Geophys. Res.*, *112*, C09013, doi:10.1029/2006JC003759.

Bates, N. R., and A. J. Peters (2007), The contribution of atmospheric acid deposition to ocean acidification in the subtropical North Atlantic Ocean, *Mar. Chem.*, *107*, 547–558.

Bates, N. R., A. F. Michaels, and A. H. Knap (1996a), Alkalinity changes in the Sargasso Sea: Geochemical evidence of calcification?, *Mar. Chem.*, *51*(4), 347–358.

Bates, N. R., A. F. Michaels, and A. H. Knap (1996b), Seasonal and interannual variability of the oceanic carbon dioxide system at the U.S. JGOFS Bermuda Atlantic Time-Series Site, *Deep Sea Res., Part II*, *43*(2-3), 347–383.

Bates, N. R., L. Samuels, and L. Merlivat (2001), Biogeochemical and physical factiors infuencing seawater fCO_2 and air-sea CO_2 exchange on the Bermuda coral reef, *Limnol. Oceanogr.*, *46*(4), 833–846.

Berelson, W., W. Balch, R. Feely, C. Sabine, K. Lee, and R. Najjar (2007), Relating estimates of $CaCO_3$ dissolution in the water column to measurements of $CaCO_3$ rain into sediment traps and dissolution on the sea floor, *Global Biogeochem. Cycles*, *21*, GB1024, doi:10.1029/2006GB002803.

Bissinger, J. E., D. J. S. Montagnes, J. Sharples, and D. Atkinson (2008), Predicting marine phytoplankton maximum growth rates from temperature: Improving on the Eppley curve using quantile regression, *Limnol. Oceanogr.*, *53*(2), 487–493.

Boyd, P. W., et al. (2007), Mesoscale iron enrichment experiments 1993-2005: Synthesis and future directions, *Science*, *315*, 612–617.

Boyd, P. W., R. Strzepek, F. Fu, and D. A. Hutchins (2010), Environmental control of open-ocean phytoplankton groups: Now and in the future, *Limnol. Oceanogr.*, *55*(3), 1353–1376.

Boyd, P., J. LaRoche, M. Gall, R. Frew, and R. M. L. McKay (1999), Role of iron, light, and silicate in controlling algal biomass in subantarctic waters SE of New Zealand, *J. Geophys. Res.*, *104*, 13,395–13,408, doi:10.1029/1999JC900009.

Brand, L. E. (1991), Minimum iron requirements of marine phytoplankton and the implications for the biogeochemiocal control of new production, *Limnol. Oceanogr.*, *36*, 1756–1771.

Bruland, K. W., R. P. Franks, G. A. Knauer, and J. H. Martin (1979), Sampling and analytical methods for the determination of copper, cadmium, zinc, and nickel at the nanogram per liter level in sea water, *Anal. Chim. Acta*, *105*, 233–245.

Brzezinski, M. (1985), The Si:C:N ratio of marine diatoms: Interspecific variability and the effect of some environmental variables, *J. Phycol.*, *21*, 347–357.

Brzezinski, M. A., and D. M. Nelson (1989), Seasonal changes in the silicon cycle within a Gulf Stream warm-core ring, *Deep Sea Res., Part I*, *36*, 1009–1030.

Caperon, J. (1967), Population growth in micro-organisms limited by food supply, *Ecology*, *48*, 715–722.

Carter, B. R., J. R. Toggweiler, R. M. Key, and J. L. Sarmiento (2014), Processes determining the marine alkalinity and calcium carbonate saturation state distributions, *Biogeosciences*, *11*, 7349–7362, doi:10.5194/bg-7311-7349-2014.

Crawford, D. W., et al. (2003), Influence of zinc and iron enrichments on phytoplankton growth in the northeastern subarctic Pacific, *Limnol. Oceanogr.*, *48*(4), 1583–1600.

Cutter, G., P. Andersson, L. Codispoti, P. Croot, R. Francois, M. Lohan, H. Obata, and M. R. Vab Der Loeff (2010), Sampling and sample-handling protocols for GEOTRACES cruises. [Available at www.geotraces.org.]
de Baar, H. J. W., J. T. M. de Jong, D. C. E. Bakker, B. M. Löscher, C. Veth, U. Bathman, and V. Smetecek (1995), Importance of iron for plankton blooms and carbon dioxide drawdown in the Southern Ocean, *Nature*, *373*, 412–415.
Dickson, A. G., C. L. Sabine, and J. R. Christian (2007), *Guide to Best Practices for Ocean CO_2 Measurements*, *Rep. PICES Spec. Publ. 3*, North Pac. Mar. Sci. Organ., Sidney, British Columbia.
Dugdale, R. C. (1967), Nutrient limitation in the sea: Dynamics, identification, and significance, *Limnol. Oceanogr.*, *12*, 685–695.
Dugdale, R. C., and J. J. MacIsacc (1971), A computation model for the uptake of nitrate in the Peru upwelling region, *Inv. Pesq.*, *35*(1), 299–308.
Egge, J. K., and D. L. Aksnes (1992), Silicate as regulating nutrient in phytoplankton competition, *Mar. Ecol. Prog. Ser.*, *83*(2-3), 281–289.
Eppley, R. W. (1972), Temperature and phytoplankton growth in the sea, *Fish. Bull.*, *70*, 1063–1085.
Eppley, R. W., and W. H. Thomas (1969), Comparison of half-saturation constants for growth and nitrate uptake of marine phytoplankton, *J. Phycol.*, *5*(4), 375–379.
Eppley, R. W., J. N. Rogers, and J. J. McCarthy (1969), Half-saturation constants for uptake of nitrate and ammonium by marine phytoplankton, *Limnol. Oceanogr.*, *14*(6), 912–920.
Eynaud, F., J. Giraudeau, J.-J. Pichon, and C. J. Pudsey (1999), Sea-surface distribution of coccolithophores, diatoms, silicoflagellates and dinoflagellates in the South Atlantic Ocean during the late austral summer 1995, *Deep Sea Res., Part I*, *46*, 451–482.
Feely, R. A., C. L. Sabine, K. Lee, W. Berelson, J. Kleypas, V. J. Fabry, and F. J. Millero (2004), Impact of anthropogenic CO_2 on the $CaCO_3$ system in the oceans, *Science*, *305*, 362–366.
Francois, R., S. Honjo, R. Krishfield, and S. Manganini (2002), Factors controlling the flux of organic carbon to the bathypelagic zone of the ocean, *Global Biogeochem. Cycles*, *16*(4), 1087, doi:10.1029/2001GB001722.
Freeman, N. M., and N. S. Lovenduski (2015), Decreased calcification in the Southern Ocean over the satellite record, *Geophys. Res. Lett.*, *42*, 1834–1840, doi:10.1002/2014GL062769.
Fry, C. H., T. Tyrrell, M. P. Hain, N. R. Bates, and E. P. Achterberg (2015), Analysis of global surface ocean alkalinity to determine controlling processes, *Mar. Chem.*, *174*, 46–57.
Garcia, C. A. E., V. M. T. Garcia, A. I. Dogliotti, A. Ferreira, S. I. Romero, A. Mannino, M. S. Souza, and M. M. Mata (2011), Environmental conditions and bio-optical signature of a coccolithophorid bloom in the Patagonian shelf, *J. Geophys. Res.*, *116*, C03025, 1–17, doi:10.1029/2010JC006595.
Gordon, H. R., G. C. Boynton, W. M. Balch, S. B. Groom, D. S. Harbour, and T. J. Smyth (2001), Retrieval of coccolithophore calcite concentration from SeaWiFS imagery, *Geochem. Res. Lett.*, *28*(8), 1587–1590.
Holligan, P. M., A. Charalampopoulou, and R. Hutson (2010), Seasonal distributions of the coccolithophore, *Emiliania huxleyi*, and of particulate inorganic carbon in surface waters of the Scotia Sea, *J. Mar. Syst.*, *82*(4), 195–205.
Iglesias-Rodríguez, M. D., C. W. Brown, S. C. Doney, J. Kleypas, D. Kolber, Z. Kolber, P. K. Hayes, and P. G. Falkowski (2002), Representing key phytoplankton functional groups in ocean carbon cycle models: Coccolithophorids, *Global Biogeochem. Cycles*, *16*(4), 1100, doi:10.1029/2001GB001454.
Jaccard, S. L., C. T. Hayes, A. Martínez-Garcia, D. A. Hodell, R. F. Anderson, D. M. Sigman, and G. H. D.-M. Haug (2013), Two modes of change in Southern Ocean productivity over the past million years, *Science*, *339*, 1419–1423, doi:10.1126/science.1227545.
JGOFS (1996), Protocols for the Joint Global Ocean Flux Study (JGOFS) core measurements, in *Report no. 19 of the Joint Global Ocean Flux Study*, edited by A. Knap, pp. 170, Scientific Comm. on Oceanic Res., Int. Council of Scientific Unions, Intergovernmental Oceanogr. Comm., Bergen, Norway.
Klaas, C., and D. E. Archer (2002), Association of sinking organic matter with various types of mineral ballast in the deep sea: Implications for the rain ratio, *Global Biogeochem. Cycles*, *16*(4), 1116, doi:10.1029/2001GB001765.
Knap, A. H., et al. (1993), *Bermuda Atlantic Time-Series Study—BATS: Method Manual*, *Rep. version 3*, pp. 108, US JGOFS Plann. and Coordination Off., Woods Hole Oceanogr. Inst., Woods Hole, Mass.
Kwon, E. Y., F. Primeau, and J. L. D.-S. D.-N. Sarmiento (2009), The impact of remineralization depth on the air-sea carbon balance, *Nat. Geosci.*, *2*(9), 630–635.
Lam, P. J., P. D. Tortell, and F. M. M. Morel (2001), Differential effects of iron additions on organic and inorganic carbon production by phytoplankton, *Limnol. Oceanogr.*, *46*(5), 1199–1202.
Lam, P. J., M. E. Auro, and D. C. Ohnemus (2012), Size-fractionated particle mass and composition during the U.S. GEOTRACES North Atlantic Zonal Transect, paper presented at Goldschmidt 2012, Montreal, Canada.
Leblanc, K., et al. (2009), Distribution of calcifying and silicifying phytoplankton in relation to environmental and biogeochemical parameters during the late stages of the 2005 North East Atlantic Spring Bloom, *Biogeosciences*, *6*, 2155–2179.
Le Moigne, F. A. C., R. J. Sanders, M. Villa-Alfageme, A. P. Martin, K. Pabortsava, H. Planquette, P. J. Morris, and S. J. Thomalla (2012), On the proportion of ballast versus non-ballast associated carbon export in the surface ocean, *Geophys. Res. Lett.*, *39*, L15610, doi:10.11029/12012gl052980.
Longhurst, A. R. (1998), *Ecological Geography of the Sea*, Academic Press, San Diego, Calif.
Lourantou, A., and N. Metzl (2011), Decadal evolution of carbon sink within a strong bloom area in the subantarctic zone, *Geophys. Res. Lett.*, *38*, L23608, doi:10.1029/2011GL049614.
Marra, J. F., V. P. Lance, R. D. Vaillancourt, and B. R. Hargreaves (2014), Resolving the ocean's euphotic zone, *Deep Sea Res., Part II*, *83*, 45–50.
Martínez-Garcia, A., A. Rosell-Melé, W. Geibert, R. Gersonde, P. Masqué, V. Gaspari, and C. Barbante (2009), Links between iron supply, marine productivity, sea surface temperature, and CO_2 over the last 1.1 Ma, *Paleoceanography*, *24*, PA1207, doi:10.1029/2008PA001657.
Martínez-Garcia, A., D. M. Sigman, H. Ren, R. F. Anderson, M. Straub, D. A. Hodell, S. L. Jaccard, T. I. Eglinton, and G. H. Haug (2014), Iron fertilization of the subantarctic ocean during the Last Ice Age, *Science*, *343*, 1347–1350, doi:10.1126/science.1246848.
Matsumoto, K., J. L. Sarmiento, and M. A. Brzezinski (2002), Silicic acid leakage from the Southern Ocean: A possible explanation for glacial atmospheric pCO_2, *Global Biogeochem. Cycles*, *16*(3), 1031, doi:10.1029/2001GB001442.
Menden-Deuer, S., and E. Lessard (2000), Carbon to volume relationships for dinoflagellates, diatoms, and other protist plankton, *Limnol. Oceanogr.*, *45*(3), 569–579.
Millero, F. J. (1996), *Chemical Oceanography*, 2nd ed., CRC Press, New York.
Milliman, J. (1993), Production and accumulation of calcium carbonate in the ocean: Budget of a nonsteady state, *Global Biogeochem. Cycles*, *7*, 927–957, doi:10.1029/93GB02524.
Minas, H. J., and M. Minas (1992), Net community production in "high nutrient-low chlorophyll" waters of the tropical and Antarctic oceans: Grazing vs iron hypothesis, *Oceanol. Acta*, *15*(2), 145–162.

Mobley, C. D. (1994), *Light and Water: Radiative Transfer in Natural Waters*, pp. 592, Academic Press, New York.
Moore, C. M., A. E. Hickman, A. J. Poulton, S. Seeyave, and M. I. Lucas (2007), Iron-light interactions during the CROZet natural iron bloom and EXport experiment (CROZEX): II—Taxonomic responses and elemental stoichiometry, *Deep Sea Res.*, *54*, 18–20.
Moore, C. M., et al. (2013), Processes and patterns of oceanic nutrient limitation, *Nat. Geosci.*, *6*(9), 701–710.
Moore, T. S., M. D. Dowell, and B. A. Franz (2012), Detection of coccolithophore blooms in ocean color satellite imagery: A generalized approach for use with multiple sensors, *Remote Sens. Environ.*, *117*, 249–263.
Morse, J. W., and F. T. Mackenzie (1990), *Geochemistry of Sementary Carbonates*, Elsevier Scientific Publishing Co., New York.
Nielsdottir, M. C., C. M. Moore, R. Sanders, D. J. Hinz, and E. P. Achterberg (2009), Iron limitation of the postbloom phytoplankton communities in the Iceland Basin, *Global Biogeochem. Cycles*, *23*, GB3001, doi:10.1029/2008GB003410.
Ohnemus, D. C., and P. J. Lam (2014), Cycling of lithogenic marine particulates in the US GEOTRACES North Atlantic Zonal Transect, *Deep Sea Res., Part II*, *116*, 283–302.
Orsi, A., T. I. Whitworth, and W. D. Nowlin (1995), On the meridional extent and fronts of the Antarctic Circumpolar Current, *Deep Sea Res., Part I*, *42*(5), 641–673.
Owens, S. A., S. Pike, and K. O. Buesseler (2015), Thorium-234 as a tracer of particle dynamics and upper ocean export in the Atlantic Ocean, *Deep-Sea Res. Part II: Topical Studies Oceanogr.*, *116*, 42–59.
Paasche, E. (1973a), Silicon and the ecology of marine plankton diatoms. II. Silicate-uptake kinetics in five diatom species, *Mar. Biol.*, *19*, 262–269.
Paasche, E. (1973b), Silicon and the ecology of marine planktonic diatoms. 1. *Thalassiosira pseudonana* (*Cyclotella nana*) grown in chemostats with silicate as the limiting nutrient, *Mar. Biol.*, *19*, 117–126.
Paasche, E., and S. Brubak (1994), Enhanced calcification in the coccolithophorid *Emiliania huxleyi* (*Haptophyceae*) under phosphorus limitation, *Phycologia*, *33*, 324–330.
Painter, S. C., A. J. Poulton, J. T. Allen, R. Pidcock, and W. M. Balch (2010), The COPAS'08 expedition to the Patagonian Shelf: Physical and environmental conditions during the 2008 coccolithophore bloom, *Cont. Shelf Res.*, *30*(18), 1907–1923.
Parslow, J. S., P. J. Harrison, and P. A. Thompson (1984), Saturated uptake kinetics: Transient response of the marine diatom *Thalassiosira pseudonana* to ammonium, nitrate, silicate or phosphate starvation, *Mar. Biol.*, *83*(1), 51–59.
Pfeil, B., et al. (2013), A uniform, quality controlled Surface Ocean CO_2 Atlas (SOCAT), *Earth System Sci. Data*, *5*(1), 125–143.
Pike, S. M., K. O. Buesseler, J. Andrews, and N. Savoye (2005), Quantification of Th-234 recovery in small volume sea water samples by inductively coupled plasma-mass spectrometry, *J. Radioanal. Nucl. Chem.*, *263*(2), 355–360.
Pinsonneault, A. J., H. D. Matthews, E. D. Galbraith, and A. Schmittner (2012), Calcium carbonate production response to future ocean warming and acidification, *Biogeosciences*, *9*(6), 2351–2364.
Planquette, H., et al. (2007), Dissolved iron in the vicinity of the Crozet Islands, Southern Ocean, *Deep Sea Res., Part II*, *54*(18–20), 1999–2019.
Pollard, R. T., H. J. Venables, J. F. Read, and J. T. Allen (2007a), Large-scale circulation around the Crozet Plateau controls an annual phytoplankton bloom in the Crozet Basin, *Deep Sea Res., Part II*, *54*, 1915–1929.
Pollard, R., R. Sanders, M. Lucas, and P. Statham (2007b), The Crozet Natural Iron Bloom and Export Experiment (CROZEX), *Deep Sea Res., Part II*, *54*(18–20), 1905–1914.
Poulton, A. J., R. Sanders, P. M. Holligan, T. Adey, M. Stinchcombe, L. Brown, and K. Chamberlain (2006), Phytoplankton mineralisation in the tropical and subtropical Atlantic Ocean, *Global Biogeochem. Cycles*, *20*, GB4002, doi:10.1029/2006GB002712.
Poulton, A. J., A. Charalampopoulou, J. R. Young, G. A. Tarran, M. I. Lucas, and G. D. Quartly (2010), Coccolithophore dynamics in non-bloom conditions during late summer in the central Iceland Basin (July–August 2007), *Limnol. Oceanogr.*, *55*(4), 1601–1613.
Poulton, A. J., S. C. Painter, J. R. Young, N. R. Bates, B. C. Bowler, D. T. Drapeau, E. Lyczkowski, and W. M. Balch (2013), The 2008 *Emiliania huxleyi* bloom along the Patagonian Shelf: Ecology, biogeochemistry and cellular calcification, *Global Biochemical Cycles*, *27*, 1–11, doi:10.1002/2013GB004641.
Read, J. F., R. T. Pollard, and J. T. Allen (2007), Sub-mesoscale structure and the development of an eddy in the Subantarctic Front north of the Crozet Islands, *Deep Sea Res., Part II*, *54*, 1930–1948, doi:10.1016/j.dsr1932.2007.1906.1013.
Rembauville, M., J. Meilland, P. Ziveri, R. Schiebel, S. Blain, and I. Salter (2016), Planktic foraminifer and coccolith contribution to carbonate export fluxes over the central Kerguelen Plateau, *Deep Sea Res., Part I*, *111*, 91–101.
Ridgwell, A., I. Zondervan, J. C. Hargreaves, J. Bijma, and T. M. Lenton (2007), Assessing the potential long-term increase of oceanic fossil fuel CO_2 uptake due to CO_2-calcification feedback, *Biogeosciences*, *4*(4), 381–492.
Riebesell, U., I. Zondervan, B. Rost, P. D. Tortell, R. E. Zeebe, and F. M. M. Morel (2000), Reduced calcification of marine plankton in response to increased atmospheric CO_2, *Nature*, *407*(6802), 364–366.
Riebesell, U., A. Kortzinger, and A. Oschlies (2009), Sensitivities of marine carbon fluxes to ocean change, *Proc. Natl. Acad. Sci. U.S.A.*, *106*(49), 20,602–20,609.
Riley, J. S., R. Sanders, C. Marsay, F. A. C. Le Moigne, E. P. Achterberg, and A. J. D.-G. Poulton (2012), The relative contribution of fast and slow sinking particles to ocean carbon export, *Global Biogeochem. Cycles*, *26*, GB1026, doi:10.1029/2011GB004085.
Robbins, L. L., M. E. Hansen, J. A. Kleypas, and S. C. Meylan (2010), *CO2calc: A User-Friendly Seawater Carbon Calculator for Windows, Mac OS X, and iOS (iPhone)*, pp. 17, *U.S. Geol. Surv.*, Reston, Va.
Robertson, J. E., C. Robinson, D. R. Turner, P. Holligan, A. J. Watson, P. Boyd, E. Fernandez, and M. Finch (1994), The impact of a coccolithophore bloom on oceanic carbon uptake in the northeast Atlantic during summer 1991, *Deep Sea Res., Part I*, *41*(2), 297–314.
Robinson, C., P. Holligan, T. Jickells, and S. Lavender (2009), The Atlantic Meridional Transect Programme (1995-2012), *Deep Sea Res., Part II*, *56*(15), 895–898.
Rosengard, S. Z., P. J. Lam, W. M. Balch, M. E. Auro, S. M. Pike, D. T. Drapeau, and B. C. Bowler (2015), Carbon export and transfer to depth across the Southern Ocean Great Calcite Belt, *Biogeosciences*, *12*, 3953–3971.
Salter, I., R. Schiebel, P. Ziveri, A. Movellan, R. Lampitt, and G. A. Wolff (2014), Carbonate counter pump stimulated by natural iron fertilization in the Polar Frontal Zone, *Nat. Geosci.*, *7*(12), 885–889.
Sarmiento, J. L., J. Dunne, A. Gnanadesikan, R. M. Key, K. Matsumoto, and R. Slater (2002), A new estimate of the $CaCO_3$ to organic carbon export ratio, *Global Biogeochem. Cycles*, *16*(4), 1107, doi:10.1029/2002GB001919.
Sarmiento, J. L., J. Simeon, A. Gnanadesikan, N. Gruber, R. M. Key, and R. Schlitzer (2007), Deep ocean biogeochemistry of silicic acid and nitrate, *Global Biogeochem. Cycles*, *21*, GB1S90, doi:10.1029/2006GB002720.
Shuter, B. (1979), A model of physiological adaptation in unicellular algae, *J. Theor. Biol.*, *78*, 519–552.
Sigman, D. M., D. C. McCorkle, and W. R. Martin (1998), The calcite lysocline as a constraint on glacial/interglacial low-latitude production changes, *Global Biogeochem. Cycles*, *12*, 409–427, doi:10.1029/98GB01184.
Smith, H. E. K. (2014), *The Contribution of Mineralising Phytoplankton to the Biological Carbon Pump in High Latitudes*, pp. 232, Univ. of Southampton, Southampton, U. K.

Smith, H. E. K., et al. (2012), Predominance of heavily calcified coccolithophores at low $CaCO_3$ saturation during winter in the Bay of Biscay, *Proc. Natl. Acad. Sci. U.S.A.*, *109*(23), 8845–8849.

Sunda, W. G., and S. A. Huntsman (1995), Iron uptake and growth limitation in oceanic and coastal phytoplankton, *Mar. Chem.*, *50*(1–4), 189–206.

Tanhua, T., N. R. Bates, and A. Körtzinger (2013), The marine carbon cycle and ocean carbon inventories, in *International Geophysics*, edited by G. Siedler et al., pp. 787–815, Academic Press, Amsterdam.

Thomalla, S. J., A. J. Poulton, R. Sanders, R. Turnewitsch, P. M. Holligan, and M. I. Lucas (2008), Variable export fluxes and efficiencies for calcite, opal, and organic carbon in the Atlantic Ocean: A ballast effect in action?, *Global Biogeochem. Cycles*, *22*, GB1010, doi:10.1029/2007GB002982.

Townsend, D. W., N. D. Rebuck, M. A. Thomas, L. Karp-Boss, and R. M. Gettings (2010), A changing nutrient regime in the Gulf of Maine, *Cont. Shelf Res.*, *30*, 820–832.

Volk, T., and M. I. Hoffert (1985), Ocean carbon pumps: Analysis of relative strengths and efficiencies in ocean-driven atmospheric pCO_2 changes, in *Carbon Dioxide and the Carbon Cycle, Archean to Present*, edited by E. T. Sundquist and W. S. Broecker, pp. 99–110, AGU, Washington, D. C.

Wollast, R. (1994), *The Relative Importance of Biomineralization and Dissolution of $CaCO_3$ in the Global Carbon Cycle*, *Rep. 2-7260-0164-5*, pp. 13–35, Musee Oceanographique, Monaco (Monaco).

Zeebe, R. E. (2012), History of seawater carbonate chemistry, atmospheric CO_2, and ocean acidification, in *Annual Review of Earth and Planetary Sciences*, edited by R. Jeanloz, pp. 141–165, Annual Reviews, Palto Alto, Calif.

Zeebe, R. E., and D. Wolf-Gladrow (2001), *CO_2 in Seawater: Equilibrium, Kinetics, Isotopes*, pp. 346, Elsevier Oceanogr. Ser., Amsterdam.

Zondervan, I., R. E. Zeebe, B. Rost, and U. Riebesell (2001), Decreasing marine biogenic calcification: A negative feedback on rising atmospheric pCO_2, *Global Biogeochem. Cycles*, *15*, 507–516, doi:10.1029/2000GB001321.